Title: Structure of a bacterial ABC transporter involved in the import of an acidic polysaccharide alginate

Authors: Yukie Maruyama[1,3,5], Takafumi Itoh[1,4,5], Ai Kaneko[1,5], Yu Nishitani[1], Bunzo Mikami[2], Wataru Hashimoto[1,*], Kousaku Murata[1,3,*]

Affiliations:

[1]Division of Food Science and Biotechnology, Graduate School of Agriculture, Kyoto University, Gokasho, Uji, Kyoto 611-0011, Japan

[2]Division of Applied Life Sciences, Graduate School of Agriculture, Kyoto University, Gokasho, Uji, Kyoto 611-0011, Japan

Contact Information:

[*]address correspondence to: E-mail: k-murata@lif.setsunan.ac.jp, whasimot@kais.kyoto-u.ac.jp

Additional Footnotes:

[3]Present address: Faculty of Science and Engineering, Setsunan University,

19 Ikedanaka-machi, Neyagawa, Osaka 572-8508, Japan

20 [4]Present address: Faculty of Biotechnology, Fukui Prefectural University, Kenjojima,

21 Matsuoka, Eiheiji-cho, Yoshida-gun, Fukui 910-1195, Japan

22 [5]Co-first author

23

24

SUMMARY

The acidic polysaccharide alginate represents a promising marine biomass for the microbial production of biofuels, although the molecular and structural characteristics of alginate transporters remain to be clarified. In *Sphingomonas* sp. A1, the ATP-binding cassette transporter AlgM1M2SS is responsible for the import of alginate across the cytoplasmic membrane. Here, we present the substrate-transport characteristics and quaternary structure of AlgM1M2SS. The addition of poly- or oligoalginate enhanced the ATPase activity of reconstituted AlgM1M2SS coupled with one of the periplasmic solute-binding proteins, AlgQ1 or AlgQ2. External fluorescence-labeled oligoalginates were specifically imported into AlgM1M2SS-containing proteoliposomes in the presence of AlgQ2, ATP, and Mg^{2+}. The crystal structure of AlgQ2-bound AlgM1M2SS adopts an inward-facing conformation. The interaction between AlgQ2 and AlgM1M2SS induces the formation of an alginate-binding tunnel-like structure accessible to the solvent. The translocation route inside the transmembrane domains contains charged residues suitable for the import of acidic saccharides.

INTRODUCTION

ATP-binding cassette (ABC) transporters are members of the largest protein superfamily and are found in all organisms (Jones and George, 2004). ABC transporters use the energy obtained from ATP hydrolysis to facilitate the translocation (import or export) of various substrates across cytoplasmic membranes. The substrates of ABC transporters range from small molecules such as ions, sugars, amino acids, vitamins, lipids, antibiotics, and drugs to large molecules (Higgins, 1992). The three-dimensional structure of several ABC transporters, including importers for vitamin B12, maltose, molybdate, methionine, and heme, and exporters involved in multidrug resistance, has recently been reported, and our knowledge on their structure–function relationships is increasing (Oldham et al., 2008; Locher, 2009; Rees et al., 2009; Oldham et al., 2011a; Slotboom, 2014). The common feature of all ABC transporters is that they comprise two transmembrane domains and two nucleotide-binding domains. The transmembrane domains comprise α-helices embedded in the membrane bilayer. The nucleotide-binding domains are responsible for energy generation through ATP hydrolysis. In addition to these components common to all ABC transporters, bacterial ABC importers require a solute-binding protein that specifically captures the substrate

at the cell surface for delivery to the appropriate ABC transporter (Hsiao et al., 1996; Spurlino et al., 1991; Wang et al., 2014; Tan et al., 2013; Sugiyama et al., 1996).

Bioethanol has garnered attention as an alternative fuel. To avoid competition with food materials, lignocellulosic biomass types such as wood, rice straw, and wheat straw have been studied for bioethanol production. However, the presence of lignin results in difficulty in hydrolyzing cellulose. In contrast, acidic polysaccharides such as alginate from seaweed biomass and pectin in primary plant cell walls can be easily extracted. The production of ethanol from alginate or seaweed (Takeda et al., 2011; Wargacki et al., 2012; Enquist-Newman et al., 2014) and pectin-rich biomass (Grohmann et al., 1998; Edwards and Doran-Peterson, 2012) has recently been reported and related studies are ongoing. Little is known about the import of such acidic polysaccharides into bacterial cells, but some components of the machinery involved in this process have been identified. TogMNAB from *Dickeya dadantii* (formerly known as *Erwinia chrysanthemi*) (Hugouvieux-Cotte-Pattat et al., 2001) and AguEFG from *Thermotoga maritima* (Nanavati et al., 2006) are ABC importers for pectin oligosaccharides. The solute sodium symporter, ToaA, from *Vibrio splendidus* (Wargacki et al., 2012), and the ABC transporter, AlgM1M2SS, from *Sphingomonas* sp.

77 A1 (strain A1) (Momma et al., 2000) are involved in alginate assimilation. However,
78 the mechanical and functional characteristics of these importers remain unclear.
79 Strain A1 assimilates alginate as a primary carbon source (Hisano et al., 1995).
80 The acidic polysaccharide alginate is produced by brown seaweeds and certain bacteria
81 and is composed of two types of uronates, β-D-mannuronate (M) and α-L-guluronate
82 (G). We previously reported ethanol production from an alginate by the genetically
83 engineered strain A1 (Takeda et al., 2011). When strain A1 assimilates alginate, a
84 mouth-like pit is formed on the cell surface (Aso et al., 2006) and alginate is
85 concentrated around the pit (Hisano et al., 1995) (Figure S1A and S1B). A cluster
86 containing the genes for an ABC transporter system and alginate lyases is crucial for
87 alginate uptake and degradation (Momma et al., 2000; Yoon et al., 2000; Hashimoto et
88 al., 2000). The expression of the gene cluster is regulated by an alginate-dependent
89 transcription factor, AlgO (Hayashi et al., 2014). Similar to other bacterial ABC
90 transporters (Locher, 2009), strain A1 ABC transporter (AlgM1M2SS) comprises two
91 transmembrane domains (heterodimer of AlgM1 and AlgM2) and two
92 nucleotide-binding domains (homodimer of AlgS). The periplasmic alginate-binding
93 proteins, AlgQ1 and AlgQ2, bind alginate and mediate the transfer of the
94 polysaccharide to AlgM1M2SS in the cytoplasmic membrane (Momma et al., 2005).

95 The AlgS or AlgM1-deficient strain A1 is unable to assimilate alginate, and it does not
96 exhibit pit formation on the cell surface (Momma et al., 2000), suggesting a relationship
97 between the ABC transporter and pit. In fact, when the strain A1 genetic segment,
98 including the ABC transporter genes (Figure S1A), was introduced into other
99 sphingomonads forming no pit, the resultant transformants were able to form pits on the
100 cell surface (Aso et al., 2006). The structure–function relationships of AlgQ1 and
101 AlgQ2 were previously characterized (Mishima et al., 2003; Momma et al., 2005;
102 Nishitani et al., 2012). AlgQ1 and AlgQ2 exhibit 76% sequence identity, and therefore,
103 have similar properties. They can interact with both polyalginates and oligoalginates,
104 regardless of the composition of the sugar residue of M and G (Momma et al., 2005;
105 Nishitani et al., 2012). However, in contrast to alginate lyases and solute-binding
106 proteins, the functional characteristics and tertiary structure of the ABC transporter
107 AlgM1M2SS remain unclear.

108 To study the mechanism of alginate uptake, we overexpressed AlgM1M2SS in
109 *Escherichia coli* cells, purified it to homogeneity, and functionally reconstituted it in
110 liposomes. The ATPase activity and transport rate of AlgM1M2SS coupled with
111 alginate-binding proteins were analyzed using reconstituted proteoliposomes. The
112 tertiary and quaternary structures of AlgM1M2SS in detergent-solubilized form and in

113 complex with AlgQ2 were also determined by X-ray crystallography.

114

115 **RESULTS**

116 **Overexpression of AlgM1M2SS in *E. coli* and Purification**

117 Overexpression systems for AlgM1M2SS with a His-tag sequence (10 His residues) at
118 the N-terminus of AlgM1 or the C-terminus of AlgM2 were constructed in *E. coli* cells
119 (Maruyama et al., 2012). Western blot analysis with an anti-His-tag antibody indicated
120 that *E. coli* produced AlgM2 with a His-tag at the C-terminus, but not AlgM1 with a
121 His-tag at the N-terminus. Of the various combinations of *E. coli* strains and vectors
122 used, *E. coli* BL21-Gold (DE3)/pLysS transformed with the vector pET21b was the
123 most suitable for AlgM1M2SS stable expression. To construct the plasmid, the strain A1
124 genome fragment encoding AlgS, AlgM1, and AlgM2, in that order, was inserted
125 between the *Nde*I and *Xho*I sites of pET21b (Figure S1A). Thus, the AlgM1M2SS
126 expressed in *E. coli* comprised the intact AlgS and AlgM1 as well as AlgM2 with a
127 His-tag at the C-terminus [AlgM2(H10)].

128 The purification scheme was optimized by screening detergents and immobilized
129 metal affinity chromatography resins. Among the various detergents tested, dodecyl
130 β-D-maltoside (DDM) was the most suitable for the solubilization of AlgM1M2SS from

E. coli cell membranes. After solubilization, AlgM1M2SS was purified to homogeneity by affinity chromatography followed by gel filtration chromatography.

Various detergents were also tested for purification. Some detergents such as n-octyl-β-D-glucopyranoside (OG), *N*,*N*-dimethyldodecylamine *N*-oxide (LDAO), 3-[(3-cholamidopropyl) dimethylammonio]-2-hydroxypropanesulfonate (CHAPSO), 3-[(3-cholamidopropyl) dimethylammonio] propanesulfonate (CHAPS), and octaethylene glycol monododecyl ether (C12E8), were unsuitable for purification. However, the transporter was successfully purified using DDM, n-undecyl-β-D-maltopyranoside (UDM), n-decyl-β-D-maltopyranoside (DM), sucrose monolaurate (SML), 5-cyclohexyl-1-hexyl-β-D-maltoside (Cymal-5), or 6-cyclohexyl-1-hexyl-β-D-maltoside (Cymal-6).

The presence of AlgS, AlgM1, and AlgM2 in the purified transporter was confirmed by sodium dodecyl sulfate (SDS)-polyacrylamide gel electrophoresis (PAGE) analysis and N-terminal amino acid sequencing. Purified AlgM1M2SS (6 mg) was obtained from 13.5 L of cultured *E. coli* cells. Six variants of the ABC transporter, AlgM1(d0)M2(H10)SS(WT), AlgM1(d0)M2(H10)SS(E160Q), AlgM1(d24)M2(H10)SS(WT), AlgM1(d24)M2(H10)SS(E160Q), AlgM1(d33)M2(H10)SS(WT), and AlgM1(d33)M2(H10)SS(E160Q), were purified and

subjected to stability tests as well as assays for ATPase and transport activity. The “d24” and “d33” variants of AlgM1 lacked the N-terminal 2^{nd}–24^{th} and 2^{nd}–33^{rd} residues, respectively. In AlgS(E160Q), Glu160 of the AlgS subunit, which is required for ATPase activity, was replaced by Gln. All variants were designed to express AlgM2 with a His-tag containing 10 His residues at the C-terminus [AlgM2(H10)]. The first four variant transporters were stable for a few months at 4°C, but AlgM1(d33)M2(H10)SS(WT) and AlgM1(d33)M2(H10)SS(E160Q) precipitated within a few days after purification.

ATPase Activity of AlgM1M2SS

The ATPase activity of purified AlgM1M2SS in the soluble form in the presence of detergents was analyzed through determination of phosphate released from ATP (Figure 1A). In the presence of a combination of Cymal-6 and CHAPSO, ATPase activity was enhanced by the addition of oligoalginates and AlgQ2. However, a marginal activity was detected in DDM, DM, or Cymal-6. The enzymatic assay in the soluble form is thought to be unsuitable due to high sensitivity to detergent variations. Thus, to measure the ATPase activity in AlgM1M2SS-containing proteoliposomes instead of that of the soluble form, three constructs of the transporter [AlgM1(d0)M2(H10)SS(WT),

AlgM1(d0)M2(H10)SS(E160Q), and AlgM1(d24)M2(H10)SS(WT)] were purified using DDM. Each purified AlgM1M2SS was reconstituted in proteoliposomes and its ATPase activity was measured (Figure 1B–D, Figure S2). Various alginates were prepared from sodium alginate (average molecular mass, 300 kDa) and were used for the assay. Sodium alginate was acid-hydrolyzed to obtain the M-rich block (PM) and the G-rich block (PG). PM and PG were separated based on their difference in solubility. Saturated alginate trisaccharides (MMM and GGG) were obtained by the acid hydrolysis of PM and PG. Unsaturated alginate trisaccharides (ΔMMM and ΔGGG) were prepared from PM and PG through the alginate lyase reaction. Structures of typical oligoalginates used in the current study are shown in Figure S1C.

The ATPase activity of AlgM1(d0)M2(H10)SS(WT) and AlgM1(d24)M2(H10)SS(WT) in the presence of AlgQ2 increased when ΔMMM was added to the reaction mixture (Figure 1B). No significant difference was observed between the two variants. On the other hand, the ATPase activity of the transporter without AlgQ2 and substrate was comparable to that with AlgQ2 in the absence of the substrate (ΔMMM) (Figure S2A). As expected, a marginal ATPase activity was detected in AlgM1(d0)M2(H10)SS(E160Q) (Figure 1B). An alternative saccharide, chitotetraose, was used as a control, and it did not induce the ATPase activity of either AlgM1M2SS

185 variants (Figure 1B). However, the activity of AlgM1(d0)M2(H10)SS(WT) increased
186 two- to five-fold by oligoalginates or PM compared to its ATPase activity in the absence
187 of alginate, which was considered 100% (Figure 1C and 1D). A smaller increase in
188 ATPase activity was observed in the presence of a polyalginate (sodium alginate).
189 AlgQ1 and AlgQ2 have been reported to strongly recognize non-reducing terminal
190 sugar residue (Momma et al., 2005; Nishitani et al., 2012) and to interact with MMM,
191 ΔMMM, GGG, and ΔGGG (Nishitani et al., 2012). As shown in Figure 1C and 1D, PG
192 had little effect on the ATPase activity of AlgM1(d0)M2(H10)SS(WT) reconstituted
193 with AlgQ1 and AlgQ2, respectively, probably because PG tends to form a higher-order
194 structure with the divalent cation present in the reaction mixture. The longer alginate,
195 ΔMMMM and ΔGGGG, also stimulated the ATPase activity of the transporter (Figure
196 S2B). Overall, both polyalginates and oligoalginates specifically stimulated the ATPase
197 activity of AlgM1M2SS. Oligoalginates had a stronger effect on the activity than
198 polyalginates (PM, PG, and sodium alginate).
199
200 **Alginate Transport Activity**
201 AlgM1(d0)M2(H10)SS(WT) was reconstituted in liposomes in the presence of ATP and
202 $MgCl_2$ and the transport activity was initiated by adding AlgQ2 and a 2-pyridylaminated

(PA)-saccharide (Figure 1E and Figure S2). Transport activities were detected when both ATP and AlgQ2 were present, but not when either of them was absent (Figure S2C). AlgM1(d0)M2(H10)SS(WT) transported PA-oligoalginates comprising either M or G with either a saturated or an unsaturated sugar residue at the non-reducing end. However, PA-chitotetraose was not transported, suggesting that AlgM1M2SS is specific for the transport of oligoalginates. Alginate tetrasaccharides were the most suitable in size for substrate import. Longer oligoalginates (8–20M and 8–20G), which were mixtures of oligomannuronates or oligoguluronates with degrees of polymerization from 8 to 20, were unexpectedly not transportable in this assay.

Overall Architecture of AlgM1M2SS in Complex with AlgQ2

To elucidate the structural basis of alginate uptake, we determined the tertiary structure of AlgM1M2SS in complex with an alginate-binding protein by using X-ray crystallography. Several combinations of proteins, detergents, and nucleotides were used in the crystallization attempts (Maruyama et al., 2012), and diffraction data of crystals derived under different conditions were collected. A crystal of AlgM1(d24)M2(H10)SS(E160Q) in complex with AlgQ2 that diffracted to 3.2 Å resolution was subjected to structural determination. The data collection and refinement

221 statistics are summarized in Table 1. The structure was initially determined by
222 molecular replacement using the coordinates of tetrasaccharide-bound AlgQ2 (PDB ID,
223 1J1N) (Mishima et al., 2003). Other subunits were also solved by molecular
224 replacement using overall structures of the *E. coli* maltose transporter MalFGK2 (PDB
225 IDs, 2R6G and 3FH6), the molybdate/tungstate transporter ModBC from
226 *Archaeoglobus fulgidus* (PDB ID, 2ONK) and *Methanosarcina acetivorans* (PDB ID,
227 3D31), and the *E. coli* methionine transporter MetNI (PDB ID, 3DHW), but failed.
228 Based on the similarity in primary structure, we used subunits of the maltose transporter
229 as search models. The N-terminal 258 residues specific for MalF were omitted from the
230 model. The structure was successfully solved (Figure S3A) using each subunit, MalF,
231 MalG, or MalK (PDB ID, 2R6G), in that order. A selenomethionine (SeMet) derivative
232 of AlgM1M2SS was also used to construct the model (Figure S3B). The overall
233 structure (Figure 2) consists of two transmembrane subunits, AlgM1 and AlgM2, in
234 complex with two copies of AlgS on one side and the alginate-binding protein AlgQ2 on
235 the other side. The topology of AlgM1 and AlgM2 (Figure S3C and S3D) reveals that
236 the transporter belongs to the type I ABC importers (Locher, 2009). Each AlgM1 and
237 AlgM2 subunit presents six transmembrane helices (helices 1, 2, 3, 4, 5, and 6), two
238 cytoplasmic helices (helices 4a and 4b), and five periplasmic helices (helices 1a, 3a, 3b,

5a, and 5b) (Figure S3C and S3D). AlgM2 presents an additional helix, 5c, on the periplasmic side. The transporter adopts an inward-facing conformation, with AlgM1 and AlgM2 open to the cytoplasm and the ATP-binding sites of the AlgS dimer widely separated. The fold of AlgM1M2SS resembles scaffolds previously observed in MalFGK2 (maltose transporter from *E. coli*) (Oldham et al., 2007), ModBC (molybdate/tungstate transporter from *M. acetivorans*) (Gerber et al., 2008), ModABC (molybdate/tungstate transporter from *A. fulgidus*) (Hollenstein et al., 2007), and MetNI (methionine transporter from *E. coli*) (Kadaba et al., 2008). Motifs that are highly conserved among ABC transporters were also found in AlgM1M2SS, such as the EA/SA motif (Glu217-Ser218-Ala219 in AlgM1 and Glu173-Ala174-Ala175 in AlgM2), the walker A motif (GXXGXGKS/T, where X is any amino acid; Gly37-Pro38-Ser39-Gly40-Cys41-Gly42-Lys43-Ser44 in AlgS), the walker B motif (ΦΦΦΦD, in which Φ is a hydrophobic residue; Val155-Phe156-Leu157-Phe158-Asp159 in AlgS), and the ABC signature motif (LSGGQ; Leu135-Ser136-Gly137-Gly138-Gln139 in AlgS). The arrangement of these conserved motifs is consistent with the arrangement observed in known ABC transporter structures.

Since a large amount of the trisaccharide (ΔMMM) was readily obtained from

257 alginate, ΔMMM was added to the crystallization drop. However, a density map
258 corresponding to the tetrasaccharide was observed in AlgQ2 (Figure 3). Because few
259 other saccharides such as tetrasaccharide and disaccharide were detected in the ΔMMM
260 solution used for crystallization by thin layer chromatography, it is likely that the
261 trisaccharides were accommodated in the two ways.
262
263 **Overall Structure of Solute-binding Protein-free AlgM1M2SS**
264 Alginate-binding protein-free AlgM1M2SS was also crystallized. The crystal was
265 obtained in the crystallization droplet containing AlgQ2 and ATP but not oligoalginate.
266 AlgQ2-free AlgM1M2SS was found to be included in the crystal through structure
267 determination. This is probably caused by difficult interaction between ligand-free
268 AlgQ2 and the transporter. The crystal structure was determined at 4.5 Å resolution by
269 molecular replacement using the coordinates of the AlgM1M2SS heterotetramer
270 determined herein (Table 1, Figure 4A). Although the density map for the AlgS dimer
271 was relatively poor, the density for the transmembrane helices of AlgM1 and AlgM2
272 was rigorously observed (Figure S4). The conformation of AlgQ2-free AlgM1M2 was
273 identical to that of the AlgQ2-bound form (Figure 4B). The root mean square deviation
274 (rmsd) among the 283 Cα atoms of the two AlgM1 subunits was 0.32 Å, and the rmsd

among the 275 Cα atoms of the two AlgM2 subunits was 0.50 Å (Table S1).

Interaction between Subunits

AlgQ2 is divided into two structural domains called the N- and C-terminal domains. Alginate binds to a deep cleft at the interface formed by the two domains. This association accompanies an inter-domain closure of approximately 30 degrees (Mishima et al., 2003). The conformation of AlgQ2 in the complex form with AlgM1M2SS is essentially identical to that observed in the previously reported structure of oligoalginate-bound AlgQ2 (Mishima et al., 2003). At the interface between AlgQ2 and AlgM1M2, helix 5c of AlgM2 protrudes considerably into the AlgQ2 side and covers half the alginate-binding cleft of AlgQ2 (Figure 2). The other half of AlgQ2 alginate-binding cleft is partially covered by AlgM1. The uncovered part of the alginate-binding cleft of AlgQ2 resembles the entrance of a tunnel that continues inside AlgQ2 (Figure 5A). AlgQ2 accommodates oligoalginate at the back of the tunnel (Figure 5B). The length of this tunnel is approximately 30 Å, corresponding to the length of alginate heptasaccharides.

AlgM1M2 interacts with AlgS primarily through helices 4a, called the conserved coupling helices (EA/SA motifs). Each coupling helix of AlgM1 or AlgM2

protrudes into a surface cleft of AlgS and lies approximately parallel to the membrane bilayer. These interaction modes are consistent with the known structures of ABC transporters.

Inner Cavity of AlgM1M2

AlgM1M2 contains a large cavity that is accessible from the cytoplasm (Figure 5C). The periplasmic end is fully closed, whereas the cytoplasmic end is slightly open and surrounded by hydrophobic amino acid residues such as Phe199, Ile202, Val203, Leu245, and Ile202 of AlgM1 and Phe155, Leu159, Leu203, Leu204, Ile207, and Phe282 of AlgM2. The distance between the periplasmic and cytoplasmic ends of this cavity is approximately 27 Å, which corresponds to approximately six residues of linear alginate. The size of the cytoplasmic end of the cavity is approximately 8 Å × 20 Å. The opening is just large enough to admit M or G of alginate.

The molecular surface of the transmembrane region that faces lipids in AlgM1M2 is hydrophobic, whereas the surface of the inner cavity is charged (Figure 6A). A positive charge is observed at the periplasmic side of the inner cavity due to residues AlgM1 Lys195 and AlgM2 Arg209. When AlgM1 and AlgM2 were superimposed onto MalF and MalG in the saccharide-binding maltose transporter (PDB

311 ID, 2R6G), respectively, the residues corresponding to the maltose-binding residues
312 were deduced (Figure 7). Similarly, in the maltose transporter, all residues near the
313 maltose were from AlgM1, but not from AlgM2. AlgM1 charged residues, Lys195,
314 Glu196, Asp200, and Arg249, are located around the putative ligand-binding site
315 deduced from the structure of MalFGK2. It is an AlgM1M2 characteristic because there
316 is no charged residue in the inner cavity of the maltose transporter whose structure
317 resembles that of AlgM1M2SS.
318 Charged residues (AlgM1 Lys195, Glu196, Asp200, Arg249, and Glu259, and
319 AlgM2 Arg209) in the cavity of AlgM1(d24)M2(H10)SS(WT), as well as histidine
320 residues (AlgM1 His141 and His252), were mutated to alanine by site-directed
321 mutagenesis. The ATPase activity and transport rate of these mutant transporters were
322 measured using AlgQ2 and PA-ΔMMMM as a substrate (Figure 8). Compared to
323 AlgM1(d24)M2(H10)SS(WT), both ATPase and transport activities of H141A and
324 E196A decreased to <50%, suggesting that replacement of His141 or Glu196 by alanine
325 disturbed the conformational change accompanying ATP hydrolysis, resulting in a
326 decrease in the substrate transport rate of these mutants. On the other hand, in E259A,
327 R209A, and E196A/E259A mutants, transport activities decreased to <40%, but ATPase
328 activities remain high (60, 80, and 103%, respectively), suggesting that the

conformational change occurred in these mutants, but the substrate was hardly transported. Because AlgM1 Glu259 and AlgM2 Arg209 are present at the periplasmic side of the inner cavity, changes in the surface charge distribution might prevent the substrate translocation in these mutants. In K195A and R249A mutants, both ATPase and transport activities decreased more moderately, whereas Asp200 and His252 mutations resulted in higher ATPase activity and 63–92% transport activity.

Structure and Function of AlgS

AlgS possesses an N-terminal ATP binding domain and an additional C-terminal domain similar to those of *E. coli* MalK and MetN, and *M. acetivorans* ModC. As shown in Table S1, tertiary structures of these transporters are very similar. However, when comparing the AlgS dimer structure to that of other ABC transporters, the values of rmsd and numbers of matching Cα atoms indicate that conformation of the AlgS dimer was mainly similar to that of the MalK dimer in the binding protein-free maltose transporter. The C-terminal domain of some ABC proteins regulates ATPase activity by interaction of transport substrate in the cell (Gerber et al., 2008; Kadaba et al., 2008). However, ATPase activity was not inhibited by increasing oligosaccharide concentration in AlgM1M2SS (Figure S2E).

DISCUSSION

The first step of alginate uptake via the ABC transporter in strain A1 is the accommodation of alginate by the periplasmic solute-binding protein AlgQ1 or AlgQ2. This step was previously investigated in detail by determining the affinity of AlgQ1 and AlgQ2 for various oligoalginates as well as their X-ray crystal structures in holo form (Momma et al., 2005; Nishitani et al., 2012). AlgQ1 and AlgQ2 recognize the non-reducing terminal residue of alginate with at least four subsites and have a broad substrate preference for M and G. The substrate specificity of the ATPase activity of reconstituted AlgM1M2SS (Figure 1) was broadly consistent with these results. Because the oligoalginate-bound form of AlgQ1 and AlgQ2 did not exhibit structural changes, depending on the type of bound alginate (Momma et al., 2005; Nishitani et al., 2012), the interaction between AlgM1M2 and the solute-binding protein is thought to be independent of the alginate type. Thus, the promotion of AlgS ATPase activity by alginate depends on the ability of the alginate-binding proteins to interact with the substrate. As shown in Figure 1C and 1D, for AlgQ1 and AlgQ2, polyalginates such as sodium alginate and PM promoted ATPase activity. Because these saccharides are much longer than the subsites of AlgQ1 and AlgQ2, and the void formed by AlgQ2 and

AlgM1M2 is too small to accommodate entire polyalginates, the tunnel-like structure that opened to the solvent (Figure 5A and 5B) suggests that non-reducing terminal residue of polyalginate trapped in the tunnel and other residues are flexible outward of the protein.

However, AlgM1M2SS substrate specificity for the transport activity is inconsistent with that of the ATPase activity (Figure 1). This may be because substrates for these assays were different. Non-labeled oligoalginate was used for ATPase activity, while PA-labeled oligoalginate was utilized for transport assay. PA-derivatized fluorescence-labeled oligoalginate with a modified reducing end sugar can be transported into the proteoliposome, suggesting that the recognition of the reducing terminal sugar is less important in the transport system. In fact, AlgM1(d24)M2(H10)SS(WT) ATPase activities using ΔMMM, ΔMMMM, and PA-ΔMMMM as substrates were comparable (Figure S2B). However, the structure of the reducing terminal residue was significantly different between non-labeled and PA-labeled oligoalginate (Figure S1C). Therefore, caution is required in interpreting the experimental results. Alginate trisaccharide transport by reconstituted AlgM1M2SS was reduced compared to tetrasaccharide transport (Figure 1E). This decreased transport may be due to a minimal interaction of alginate-binding proteins with the PA-reducing

383 terminal sugar of the trisaccharide at subsite 3. Alginates longer than heptasaccharides
384 (8–20M and 8–20G), which are longer than the length of the inner cavity of AlgM1M2
385 when the alginate adopts a linear conformation, were also not transported by
386 AlgM1M2SS. Because alginate-degrading enzymes are present in the cytoplasm in
387 strain A1 (Yonemoto et al., 1992) and strain AL-L, a strain A1 derivative with mutations
388 in the AlgS gene is unable to assimilate polyalginate (Momma et al., 2000); strain A1
389 has been thought to incorporate polyalginate into the cytoplasm. However, in the *in*
390 *vitro* assay system used in the current study, strain A1 failed to transport the
391 polysaccharide. Additional factors such as the alginate concentrator pit formed on the
392 cell surface of strain A1 (Figure S1A and S1B) may be required for macromolecular
393 transport by AlgM1M2SS.
394 Sugar transport by the maltose ABC transporter has been extensively
395 characterized. Among known structures of bacterial ABC transporters, the structure of
396 AlgM1M2SS most closely resembles the structure of the maltose ABC transporter. The
397 sequence identities of AlgM1 *vs.* MalF, AlgM2 *vs.* MalG, and AlgS *vs.* MalK are 24, 26,
398 and 53%, respectively. The conformation of AlgM1M2SS is more similar to that of the
399 resting state model of MalFGK2 without MalE (PDB ID, 3FH6) (Bordignon et al.,
400 2010) in comparison with the model of MalFGK2 in complex with MalE (PDB IDs,

2R6G and 3PV0). As shown in Figure 9, the structures of the nucleotide-binding subunits (AlgS) and coupling helix-mediated interactions between the transmembrane domains (AlgM1 and AlgM2) and nucleotide-binding domains (AlgS) are common to those of the maltose transporter and molybdate/tungstate transporter. However, the periplasmic solute-binding protein and its interaction with the transmembrane domain are specific to the individual transporter. The contact area between AlgQ2 and AlgM1M2 is smaller than that between MalE and MalFG and between ModA and ModBC and is characteristics in that helix 5c of AlgM2 protrudes into AlgQ2.

In the maltose transporter, MalFG, conformation changes upon interacting with the solute-binding protein MalE (Oldham and Chen, 2011b). In the pre-translocation model of MalFGK2 (PDB ID, 3PV0) in complex with MalE, maltose was bound to MalFG inner cavity as well as to MalE substrate-binding cleft. However, the substrate was found only in AlgQ2 in the case of AlgM1M2SS complexed with AlgQ2. In contrast to the slight, but significant conformational changes observed in the solute-binding protein-free and protein-bound MalFG, the conformation of free AlgM1M2 without the periplasmic solute-binding protein was identical to the conformation of AlgM1M2 in complex with AlgQ2 (Figure 4B), suggesting that the ABC transporter in the resting state conformation can bind solute-binding protein

without conformational change. The absence of allosteric coupling might be due to the detergent used for crystallization because the transporter was inactive in the presence of detergents such as DDM, Cymal-6, and DM (Figure 1A).

Recently, structures of MalE-bound MalFGK2 with maltoheptaose and maltopentaose have been reported (Oldham et al., 2013). In the maltose transporter, which imports maltodextrin up to the size of heptasaccharides, the reducing end of the substrate is located behind MalE and the non-reducing terminal residues are flexible in the void formed between MalE and MalFG. The reducing end of maltodextrin interacts with MalG and the modification of the reducing end prevents transport in the maltose transporter system. However, no interaction between oligoalginate and AlgM1M2 was observed in the crystal structure determined in the current study. The interaction between AlgQ2 and alginate differs from that between MalE and maltodextrin in that the non-reducing end is recognized tightly at the back of AlgQ2 cleft. The tunnel-like structure shown in Figure 5 is also specific to AlgQ2 and AlgM1M2. Since AlgQ2 enhanced the ATPase activity of the ABC transporter in the presence of alginate polysaccharide (Figure 1D), interaction of alginate hexadecasaccharide with the tunnel-like structure was simulated by using a docking program (Figure 5D). The substrate seems to be effectively accommodated at the inner space of AlgQ2 and the

interface formed between AlgQ2 and AlgM1M2, suggesting that the tunnel-like structure is suitable for import of longer oligoalginates.

An inner cavity is also observed in MalFG (PDB ID, 3FH6). The distinctive charged residues observed at the surface of the cavity of AlgM1M2 are absent in MalFG (Figure 6B). The site-directed mutagenesis study (Figure 8) suggests that the negative and positive charge, derived from Glu259 and Arg209 on the periplasmic side of AlgM1 and AlgM2, respectively (Figure 6A), may contribute to the effective passing of the negatively charged substrate from the alginate-binding protein without influencing AlgM1M2 conformational change. The correct positioning of the substrate might fail in other mutants, showing reduced ATPase and transport activities such as H141A, K195A, E196A, and R249A mutants. As a result, it might be difficult to change the conformation of such mutants upon ATP hydrolysis by AlgS.

In conclusion, the first crystal structure of the alginate uptake transporter AlgM1M2SS suggests structural determinants responsible for the transport of acidic saccharides by this ABC transporter. Although the basic scaffolds of ABC transporters are conserved regardless of the substrate, the interaction of the solute-binding protein and transmembrane domain and the surface structure of the inner cavity are specific to each substrate.

EXPERIMENTAL PROCEDURES

Protein Expression and Purification

E. coli BL21-Gold(DE3)/pLysS was used as the host strain for the expression of various types of AlgM1M2SS (Table S2). The methionine auxotrophic *E. coli* strain B834(DE3) was used to prepare SeMet-substituted AlgM1M2SS. TB medium (Tartof and Hobbs, 1987) was used to culture BL21-Gold(DE3)/pLysS and minimal medium containing SeMet (25 mg/mL) was used to culture B834(DE3). Cells were collected by centrifugation at 6,000 *g* and 4°C for 5 min, suspended in a standard buffer [20 mM Tris-HCl (pH 8.0), 100 mM NaCl, 10 mM $MgCl_2$, and 10% glycerol], and ultrasonically disrupted (Insonator Model 201M, Kubota) for 20 min on ice. The supernatant fraction obtained after centrifugation at 20,000 *g* and 4°C for 20 min to remove cell debris was further ultracentrifuged at 100,000 *g* and 4°C for 1 h. The pelleted membranes were solubilized with 1% DDM (Dojindo) and loaded on a Ni-NTA column (Qiagen). After being washed with standard buffer containing 1× critical micelle concentration (CMC) of detergent and 20 mM imidazole, the sample was eluted using a linear gradient of imidazole (20–200 mM). The proteins were confirmed by SDS-PAGE, combined, and concentrated by ultrafiltration. The sample was then applied to a HiLoad 16/60

Superdex 200 PG or Superdex 200 GL column (GE Healthcare Science) and eluted using standard buffer containing 2× CMC of detergent. Detergent exchange was performed during protein purification at the affinity chromatography step. Purified AlgM1M2SS was concentrated to a final concentration of 10 mg/mL and stored at 4°C. The AlgM1(d24)M2(H10)SS(WT) selenomethionine derivative was purified using the same method, except that 5 mM 2-mercaptoethanol was added throughout the purification process. The purified protein concentration was determined using a bicinchoninic acid protein assay kit (Pierce).

AlgQ1 and AlgQ2 were expressed and purified as previously described (Nishitani et al., 2012).

Preparation of Fluorescence-labeled Alginate Oligosaccharides

Oligoalginates were derivatized with 2-aminopyridine (2-AP), as reported previously (Ishii et al., 2001) with slight modifications. Briefly, alginate oligosaccharides (0.4%) were dissolved in 1 mL of 1.0 M $NaCNBH_3$ (Wako Pure Chemical Industries) and 0.5 M 2-AP (Wako Pure Chemical Industries), then incubated at 40°C for 20 h. The pH of the solution was adjusted to 5.8 with 10% acetic acid before incubation. The reaction mixture was applied to a Bio gel P2 column to remove unreacted 2-AP. The column was developed with distilled water. The absorbance of the eluent was monitored at 300 nm

to detect 2-AP and PA-saccharides. The UV-positive fractions were pooled and confirmed by TLC. Freeze-dried oligosaccharides were dissolved in 50 mM ammonium bicarbonate and applied to a HiTrapQ HP column (GE Healthcare Science). Oligosaccharides were eluted using a linear gradient of 50–500 mM ammonium bicarbonate. Fractions containing PA-oligosaccharides were confirmed by TLC and freeze-dried to remove ammonium bicarbonate.

Preparation of Proteoliposomes

Soybean L-α-phosphatidylcholine (Type II-S, Sigma) was dissolved in chloroform at a concentration of 33 mg/mL. Chloroform was removed by rotary evaporation (N-1000-WD, Eyela), and any residual solvent was removed under vacuum for 3 h. The dried lipids were then hydrated by incubation at 50 mg/mL in 20 mM Tris-HCl (pH 8.0) with 1 mM dithiothreitol at room temperature. The solution was sonicated three times on ice using a rod sonicator (Sonics & Materials). The hydrated lipid solution was frozen in liquid nitrogen and thawed at 37°C. After seven rounds of freezing and thawing, the liposome solution was stored at −80°C.

The lipids were thawed in a water bath at 37°C before use and extruded 17 times through a 100 nm polycarbonate membrane using a Mini-Extruder (Avanti Polar Lipids). Purified AlgM1M2SS [at a 1:80 ratio (w/w) of protein/lipids] and OG (final

509 1.4%) were added to the mixture. The mixture was equilibrated at room temperature for
510 10 min. The solution was diluted 30 fold with 20 mM Tris-HCl (pH 8.0) and incubated
511 on ice for 1 h.

512 **Assay for ATPase Activity and Alginate Transport**

513 The ATPase activity of AlgM1M2SS-containing proteoliposomes was measured in
514 200-μL reaction mixtures containing 1.3 mg/mL lipids, 0.1 μM AlgM1M2SS, 1.3 μM
515 AlgQ1 or AlgQ2, 20 mM Tris-HCl (pH 8.0), 2 mM ATP, 10 mM $MgCl_2$, and alginate
516 polysaccharides or oligosaccharides. The reaction mixtures were incubated at 37°C.
517 Samples (30 μL) were removed at various time points and added to 30 μL of 12% SDS
518 to stop the reaction. Inorganic phosphate was then assayed colorimetrically (Chifflet et
519 al., 1988). ATPase activity was represented as phosphate (nmol) produced by 1 mg
520 AlgM1M2SS per 1 min. To measure the uptake of alginate, ATP and $MgCl_2$ (each at a
521 final concentration of 5 mM) were added to the proteoliposomes. The mixture was
522 frozen in liquid nitrogen and thawed in a water bath at 20°C. The freeze and thaw cycle
523 was repeated three times to incorporate all components into the vesicle lumen and the
524 mixture was then extruded five times through a 100 nm polycarbonate membrane using
525 a Mini-Extruder (Avanti Polar Lipids). The proteoliposome mixtures were
526 ultracentrifuged at 150,000 *g* and 4°C for 30 min. The precipitated proteoliposomes

were then resuspended in 20 mM Tris-HCl (pH 8.0). Alginate-binding protein and PA-oligoalginate were added to begin the transport reaction. The final concentrations in the transport reaction were 1.3 mg/mL lipids, 0.1 μM AlgM1M2SS, 20 μM of each PA-alginate oligosaccharide, and 1 μM alginate-binding protein, in a total volume of 600 μL. The reaction mixtures were incubated at 37°C for 60 min and the proteoliposomes were recovered by ultracentrifugation at 150,000 *g* and 4°C for 15 min. The resulting precipitants were rinsed and resuspended in distilled water. The concentration of PA-oligoalginates incorporated into the liposomes was estimated by the fluorescence intensity (Ex, 310 nm; Em, 380 nm) after subtracting the value measured using liposomes without the ABC transporter.

AUTHOR CONTRIBUTIONS

YM, TI, AK, YN, and WH performed the experiments. YM, TI, AK, YN, BM, WH, and KM analyzed the data. YM, TI, WH, and KM designed the study and wrote the manuscript.

ACCESSION NUMBERS

The coordinates and structure factors for solute-binding protein-free and AlgQ2-bound AlgM1M2SS have been deposited in the Protein Data Bank, www.pdb.org (PDB entries

4TQV and 4TQU).

SUPPLEMENTAL INFORMATION

Supplemental Information includes four figures, two tables, and experimental procedures and can be found online at #######.

ACKNOWLEDGMENTS

We thank Ms. Kasumi Uenishi, Ms. Chizuru Tokunaga, Ms. Ai Matsunami, and Mr. Takuya Yokoyama for their excellent technical assistance. The synchrotron radiation experiments were performed at beamlines BL38B1, BL41XU, and BL44XU of SPring-8 with the approval of the Japanese Synchrotron Radiation Research Institute (JASRI) (Proposal Nos. 2013A1106, 2012B1265, 2012A1317, 2011B1108, 2011B2055, 2011A1186, 2010B6500, 2010A1279, and 2009B1177). This work was supported in part by Grants–in-Aid for Scientific Research from the Japanese Society for the Promotion of Science and Targeted Proteins Research Program from Ministry of Education, Culture, Sports, Science, and Technology in Japan (BM, WH, and KM).

REFERENCES

561 Aso, Y., Miyamoto, Y., Harada, K.M., Momma, K., Kawai, S., Hashimoto, W., Mikami,
562 B., and Murata, K. (2006). Engineered membrane superchannel improves
563 bioremediation potential of dioxin-degrading bacteria. Nat. Biotechnol. *24*, 188–189.

564 Baker, N.A., Sept, D., Joseph, S., Holst, M. J., and McCammon, J. A. (2001).
565 Electrostatics of nanosystems: application to microtubules and the ribosome. Proc.
566 Natl. Acad. Sci. USA *98*, 10037–10041.

567 Bordignon, E., Grote, M., and Schneider, E. (2010). The maltose ATP-binding cassette
568 transporter in the 21st century--towards a structural dynamic perspective on its mode
569 of action. Mol. Microbiol. *77*, 1354–1366.

570 Chifflet, S., Torriglia, A., Chiesa, R., and Tolosa, S. (1988). A method for the
571 determination of inorganic phosphate in the presence of labile organic phosphate and
572 high concentrations of protein: application to lens ATPases. Anal. Biochem. *168*,
573 1–4.

574 Edwards, M.C., and Doran-Peterson, J. (2012). Pectin-rich biomass as feedstock for fuel
575 ethanol production. Appl. Microbiol. Biotechnol. *95*, 565–575.

576 Enquist-Newman, M., Faust, A.M., Bravo, D.D., Santos, C.N., Raisner, R.M., Hanel, A.,
577 Sarvabhowman, P., Le, C., Regitsky, D.D., Cooper, S.R., et al. (2014). Efficient
578 ethanol production from brown macroalgae sugars by a synthetic yeast platform.
579 Nature *505*, 239–243.

580 Gerber, S., Comellas-Bigler, M., Goetz, B.A., and Locher, K.P. (2008). Structural basis
581 of trans-inhibition in a molybdate/tungstate ABC transporter. Science *321*, 246–250.

582 Grohmann, K., Manthey, J.A., Cameron, R.G., and Buslig, B.S. (1998). Fermentation of
583 galacturonic acid and pectin-rich materials to ethanol by genetically modified strains
584 of *Erwinia*. Biotechnol. Lett. *20*, 195–200.

585 Hashimoto, W., Miyake, O., Momma, K., Kawai, S., and Murata, K. (2000). Molecular
586 identification of oligoalginate lyase of *Sphingomonas* sp. strain A1 as one of the
587 enzymes required for complete depolymerization of alginate. J. Bacteriol. *182*,
588 4572–4577.

589 Hayashi, C., Takase, R., Momma, K., Maruyama, Y., Murata, K., and Hashimoto, W.
590 (2014). Alginate-dependent gene expression mechanism in *Sphingomonas* sp. strain
591 A1. J. Bacteriol. *196*, 2691–2700.

592 Higgins, C.F. (1992). ABC transporters: from microorganisms to man. Annu. Rev. Cell
593 Biol. *8*, 67–113.

594 Hisano, T., Yonemoto, Y., Yamashita, T., Fukuda, Y., Kimura, A., and Murata, K.
595 (1995). Direct uptake of alginate molecules through a pit on the bacterial cell
596 surface: A novel mechanism for the uptake of macromolecules. J. Ferment. Bioeng.
597 *79*, 538–544.

598 Hisano, T., Kimura, N., Hashimoto, W., and Murata, K. (1996). Pit structure on
599 bacterial cell surface. Biochem. Biophys. Res. Commun. *220*, 979–982.

600 Hollenstein, K., Frei, D.C., and Locher, K.P. (2007). Structure of an ABC transporter in
601 complex with its binding protein. Nature *446*, 213–216.

602 Hsiao, C.D., Sun, Y.J., Rose, J., and Wang, B.C. (1996). The crystal structure of
603 glutamine-binding protein from *Escherichia coli*. J. Mol. Biol. *262*, 225–242.

604 Hugouvieux-Cotte-Pattat, N., Blot, N., and Reverchon, S. (2001). Identification of
605 TogMNAB, an ABC transporter which mediates the uptake of pectic oligomers in
606 *Erwinia chrysanthemi* 3937. Mol. Microbiol. *41*, 1113–1123.

607 Ishii, T., Ichita, J., Matsue, H., Ono, H., and Maeda, I. (2001). Fluorescent labeling of
608 pectic oligosaccharides with 2-aminobenzamide and enzyme assay for pectin.
609 Carbohydr. Res. *337*, 1023–1032.

610 Jones, P.M., and George, A.M. (2004). The ABC transporter structure and mechanism:
611 perspectives on recent research. Cell Mol. Life. Sci. *61*, 682–699.

612 Kadaba, N.S., Kaiser, J.T., Johnson, E., Lee, A., and Rees, D.C. (2008). The
613 high-affinity *E. coli* methionine ABC transporter: structure and allosteric regulation.
614 Science *321*, 250–253.

615 Locher, K.P. (2009). Structure and mechanism of ATP-binding cassette transporters.
616 Philos. Trans. R. Soc. Lond. B Biol. Sci. *364*, 239–245.

617 Maruyama, Y., Itoh, T., Nishitani, Y., Mikami, B., Hashimoto, W., and Murata, K.
618 (2012). Crystallization and preliminary X-ray analysis of alginate importer from
619 *Sphingomonas* sp. A1. Acta Crystallogr. F Struct. Biol. Cryst. *68*, 317–320.

620 Mishima, Y., Momma, K., Hashimoto, W., Mikami, B., and Murata, K. (2003). Crystal
621 structure of AlgQ2, a macromolecule (alginate)-binding protein of *Sphingomoas* sp.

622 A1, complexed with an alginate tetrasaccharide at 1.6-Å resolution. J. Biol. Chem.
623 *278*, 6552–6559.

624 Momma, K., Okamoto, M., Mishima, Y., Mori, S., Hashimoto, W., and Murata, K.
625 (2000). A novel bacterial ATP-binding cassette transporter system that allows uptake
626 of macromolecules. J. Bacteriol. *182*, 3998–4004.

627 Momma, K., Mishima, Y., Hashimoto, W., Mikami, B., and Murata, K. (2005). Direct
628 evidence for *Sphingomoas* sp. A1 periplasmic proteins as macromolecule-binding
629 proteins associated with the ABC transporter: molecular insights into alginate
630 transport in the periplasm. Biochemistry *44*, 5053–5064.

631 Nanavati, D.M., Thirangoon, K., Noll, K.M. (2006). Several archaeal homologs of
632 putative oligopeptide-binding proteins encoded by *Thermotoga maritima* bind sugars.
633 Appl. Environ. Microbiol. *72*, 1336–1345.

634 Nishitani, Y., Maruyama, Y., Itoh, T., Mikami, B., Hashimoto, W., and Murata, K.
635 (2012). Recognition of heteropolysaccharide alginate by periplasmic solute-binding
636 proteins of a bacterial ABC transporter. Biochemistry *51*, 3622–3633.

637 Oldham, M.L., Khare, D., Quiocho, F.A., Davidson, A.L., and Chen, J. (2007). Crystal
638 structure of a catalytic intermediate of the maltose transporter. Nature *450*, 515–521.

639 Oldham, M.L., Davidson, A.L., and Chen, J. (2008). Structural insights into ABC
640 transporter mechanism. Curr. Opin. Struct. Biol. *18*, 726–733.

641 Oldham, M.L., and Chen, J. (2011a). Snapshots of the maltose transporter during ATP
642 hydrolysis. Proc. Natl. Acad. Sci. USA *108*, 15152–15156.

643 Oldham, M.L., and Chen, J. (2011b). Crystal structure of the maltose transporter in a
644 pretranslocation intermediate state. Science *332*, 1202–1205.

645 Oldham, M.L., Chen, S., and Chen, J. (2013). Structural basis for substrate specificity in
646 the *Escherichia coli* maltose transport system. Proc. Natl. Acad. Sci. USA *110*,
647 18132–18137.

648 Rees, D.C., Johnson, E., and Lewinson, O. (2009). ABC transporters: the power to
649 change. Nat. Rev. Mol. Cell Biol. *10*, 218–227.

650 Slotboom, D.J. (2014). Structural and mechanistic insights into prokaryotic
651 energy-coupling factor transporters. Nat. Rev. Microbiol. *12*, 79–87.

652 Spurlino, J.C., Lu, G.Y., and Quiocho, F.A. (1991). The 2.3-Å resolution structure of
653 the maltose- or maltodextrin-binding protein, a primary receptor of bacterial active
654 transport and chemotaxis. J. Biol. Chem. *266*, 5202–5219.

655 Sugiyama, S., Vassylyev, D.G., Matsushima, M., Kashiwagi, K., Igarashi, K., and
656 Morikawa, K. (1996). Crystal structure of PotD, the primary receptor of the
657 polyamine transport system in *Escherichia coli*. J. Biol. Chem. *271*, 9519–9525.

658 Takeda, H., Yoneyama, F., Kawai, S., Hashimoto, W., and Murata, K. (2011).
659 Bioethanol production from marine biomass alginate by metabolically engineered
660 bacteria. Energy Environ. Sci. *4*, 2575–2581.

661 Tan, K., Chang, C., Cuff, M., Osipiuk, J., Landorf, E., Mack, J.C., Zerbs, S., Joachimiak,
662 A., and Collart, F.R. (2013). Structural and functional characterization of solute
663 binding proteins for aromatic compounds derived from lignin: *p*-Coumaric acid and
664 related aromatic acids. Proteins *81*, 1709–1726.

665 Wang, S., Ogata, M., Horita, S., Ohtsuka, J., Nagata, K., and Tanokura, M. (2014). A
666 novel mode of ferric ion coordination by the periplasmic ferric ion-binding subunit
667 FbpA of an ABC-type iron transporter from *Thermus thermophilus* HB8. Acta.
668 Crystallogr. D *70*, 196–202.

669 Wargacki, A.J., Leonard, E., Win, M.N., Regitsky, D.D., Santos, C.N., Kim, P.B.,
670 Cooper, S.R., Raisner, R.M., Herman, A., Sivitz, A.B., et al. (2012). An engineered
671 microbial platform for direct biofuel production from brown macroalgae. Science
672 *335*, 308–313.

673 Yonemoto, Y., Yamaguchi, H., Kimura, A., Sakaguchi, K., Okayama, K., and Murata,
674 K. (1992). Cloning of a gene for intracellular alginate lyase in a bacterium isolated
675 from a ditch. J. Ferment. Bioeng. *73*, 225–227.

676 Yoon, H.J., Hashimoto, W., Miyake, O., Okamoto, M., Mikami, B., and Murata, K.
677 (2000). Overexpression in *Escherichia coli*, purification, and characterization of
678 *Sphingomoas* sp. A1 alginate lyases. Protein Expr. Purif. *19*, 84–90.

679

680

Figure Legends

Figure 1: *In vitro* assay of the ABC transporter AlgM1M2SS

Unless otherwise stated, saccharides were added at a final concentration of 20 μM. The error bars represent the standard error. The experiments shown in each figure were repeated three or more times using the same purification sample of the transporter. The values were obtained by subtracting the value for the liposome without the alginate importer from the value for the AlgM1M2SS-containing proteoliposome.

(A) AlgM1M2SS ATPase activity solubilized with the detergents. AlgQ2 was used as a solute-binding protein and ΔMMM as a substrate. The detergents 0.018% DDM, 0.06% Cymal-6, 0.18% DM, and a mixture of 0.045% Cymal-6 and 0.25% CHAPSO were used. The ATPase activities are represented as the release of phosphate (nmol/min) from ATP by 1 mg of AlgM1M2SS in the reaction mixture.

(B) ATPase activity of three variants of AlgM1M2SS reconstituted in liposomes with AlgQ2 and ΔMMM or chitotetraose (chito 4).

(C) Relative ATPase activity of AlgM1(d0)M2(H10)SS(WT) reconstituted in liposomes with AlgQ1 and various alginates. Alg, sodium alginate.

(D) Relative ATPase activity of AlgM1(d0)M2(H10)SS(WT) reconstituted in liposomes with AlgQ2 and various alginates.

(E) Transport rates of various ligands by AlgM1(d0)M2(H10)SS(WT) reconstituted in liposomes. AlgQ2 and various PA-labeled saccharides were added in the reaction mixture.

See also Figure S1 and S2.

Figure 2: **Structure of the ABC transporter AlgM1M2SS in complex with the periplasmic binding protein AlgQ2**

Wall-eyed stereo view of the ribbon diagram is represented. Pink, AlgQ2; blue, AlgM1; green, AlgM2; orange and cyan, AlgS. Oligomannuronate is shown as a stick model. Calcium ion is shown as a yellow ball.

See also Figure S3 and Table S1.

Figure 3: **Kicked |Fo|-|Fc| omit map around the substrate**

Density maps are contoured at 2.0 σ.

(A) Wall-eyed stereo view of density map with ΔMMMM. Subsites 1–4 are numbered.

(B) and (C) Probable ΔMMM conformations bound to AlgQ2.

Figure 4: **Structure of the binding protein-free form of the ABC transporter AlgM1M2SS**

(A) Quaternary structure of AlgM1M2SS. Wall-eyed stereo view of the ribbon diagram is represented. Blue, AlgM1; green, AlgM2; orange and cyan, AlgS.

(B) Structural comparison of AlgQ2-free and AlgQ2-bound AlgM1M2. A wall-eyed stereo view of the superimposition of binding protein-free and protein-bound AlgM1M2 is shown. Pink, AlgQ2-free AlgM1M2; light blue, AlgQ2-bound AlgM1M2. See also Figure S4.

Figure 5: **Inner spaces of the ABC transporter, AlgM1M2SS, in complex with the periplasmic binding protein AlgQ2**

(A) Surface model of AlgQ2 (pink) associated with AlgM1 (blue) and AlgM2 (green). The reducing end residue of oligomannuronate, shown as a stick model, is visible from the outside of the molecule.

(B) Tunnel-like void (meshed) formed at the interface between AlgQ2 and AlgM1.

(C) Inner space (meshed) formed by AlgM1 (blue) and AlgM2 (green). The void volume (meshed) was calculated to be 3218 $Å^3$.

(D) Docking model of AlgQ2/AlgM1M2 with hexadecamannuronate. Simulated model of oligomannuronate is represented as a stick model.

Figure 6: **Surface and charge distribution of the inner cavity**

Red, negative charge; blue, positive charge. Electronic charges were calculated using the APBS program (Baker et al., 2001).

(A) AlgM1 and AlgM2

(B) MalF and MalG from the *E. coli* maltose transporter (PDB ID, 3FH6).

Figure 7: **Structure comparison of AlgM1M2 inner cavity with that of MalFG**

(A) MalF and MalG. A maltose molecule bound in the inner cavity of MalFG (PDB ID, 2R6G) and its surrounding residues are shown as a stick model. Blue, MalF; green, MalG.

(B) AlgM1 and AlgM2 superimposed on MalF and MalG in panel A, respectively. Charged residues in AlgM1M2 inner cavity and/or the corresponding residues presented in panel A are shown as a stick model. Blue, AlgM1; and green, AlgM2.

Figure 8: **Functional analysis of AlgM1M2SS mutants**

AlgQ2 was used as a solute-binding protein and PA-ΔMMMM as a substrate. To avoid the experimental error based on the protein purification batch, each mutant transporter and wild-type AlgM1(d24)M2(H10)SS(WT) was purified and assayed in parallel. Relative ATPase activity and transport rate are represented when those of AlgM1(d24)M2(H10)SS(WT) are set as 100%. The error bars represent the standard error (n > 2).

(A) ATPase activity of AlgM1(d24)M2(H10)SS(WT) and its variants reconstituted in liposomes.

(B) Transport rate of AlgM1(d24)M2(H10)SS(WT) and its variants reconstituted in liposomes.

Figure 9: Comparison of the quaternary structure of ABC transporters

Ribbon diagrams of alginate transporter, maltose transporter (PDB ID: 3PV0), and molybdate/tungstate transporter (PDB ID: 2ONK) are shown. Bound substrates in the solute-binding protein are represented as a sphere model.

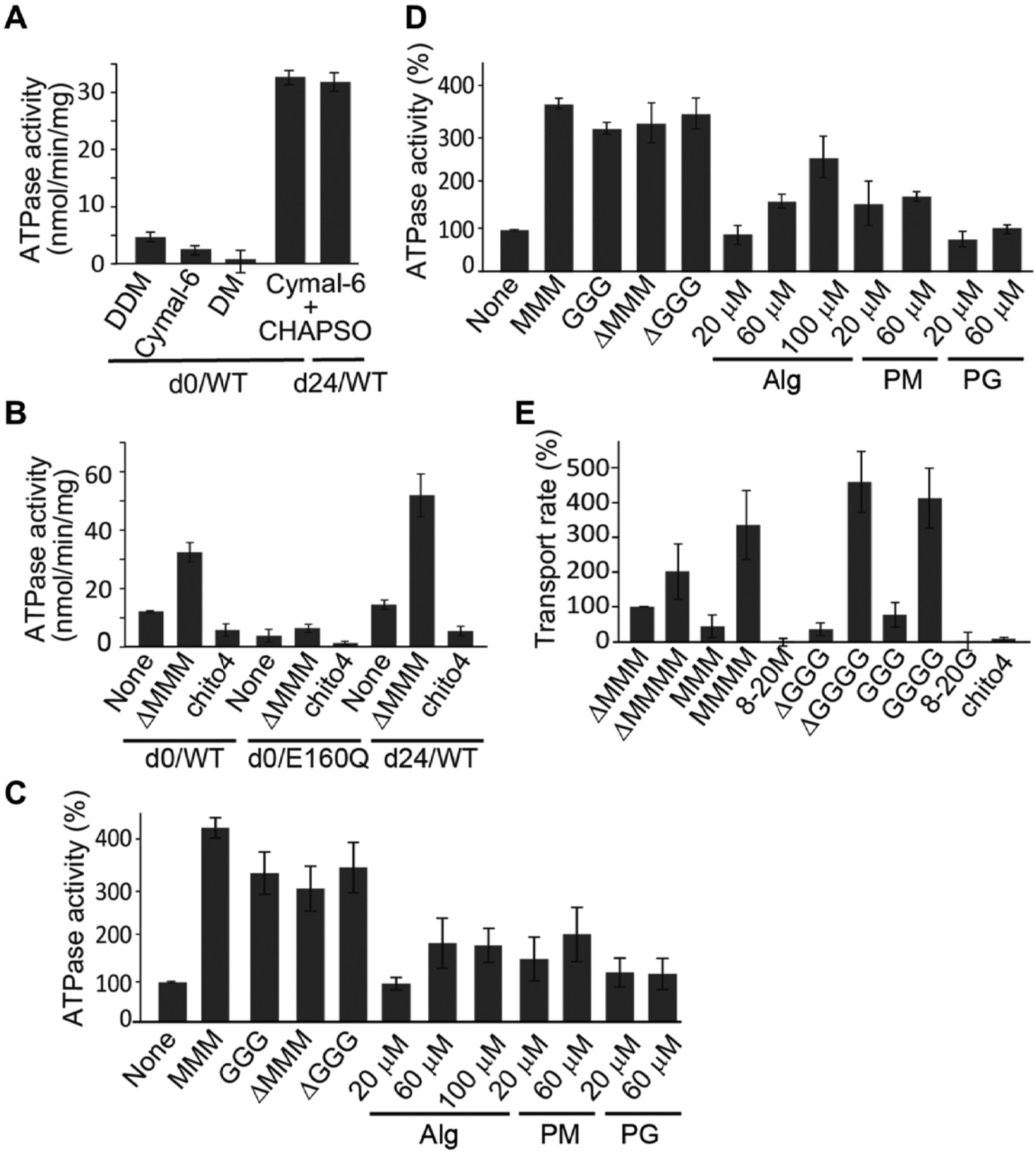
A
ATPase activity (nmol/min/mg)
0
10
20
30
DDM
Cymal-6
DM
Cymal-6 + CHAPSO
d0/WT
d24/WT
B
ATPase activity (nmol/min/mg)
0
20
40
60
None
ΔMMM
chito4
None
ΔMMM
chito4
None
ΔMMM
chito4
d0/WT
d0/E160Q
d24/WT
C
ATPase activity (%)
0
100
200
300
400
None
MMM
GGG
ΔMMM
ΔGGG
20 μM
60 μM
100 μM
20 μM
60 μM
20 μM
60 μM
Alg
PM
PG
D
ATPase activity (%)
0
100
200
300
400
None
MMM
GGG
ΔMMM
ΔGGG
20 μM
60 μM
100 μM
20 μM
60 μM
20 μM
60 μM
Alg
PM
PG
E
Transport rate (%)
0
100
200
300
400
500
ΔMMM
ΔMMMM
MMM
MMMM
8-20M
ΔGGG
ΔGGGG
GGG
GGGG
8-20G
chito4

Figure 1

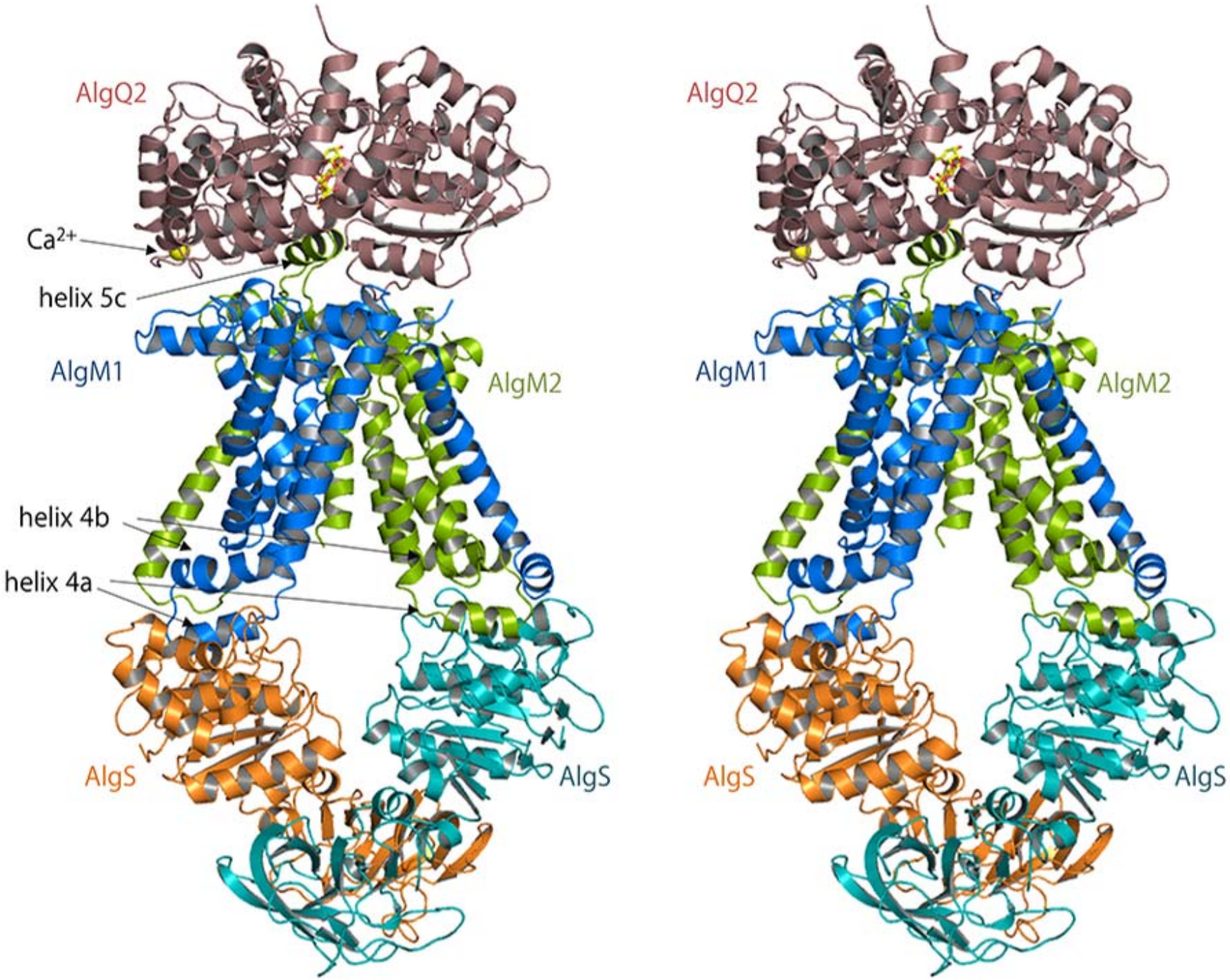
AlgQ2
Ca2+
helix 5c
AlgM1
AlgM2
helix 4b
helix 4a
AlgS
AlgS
AlgQ2
AlgM1
AlgM2
AlgS
AlgS

Figure 2

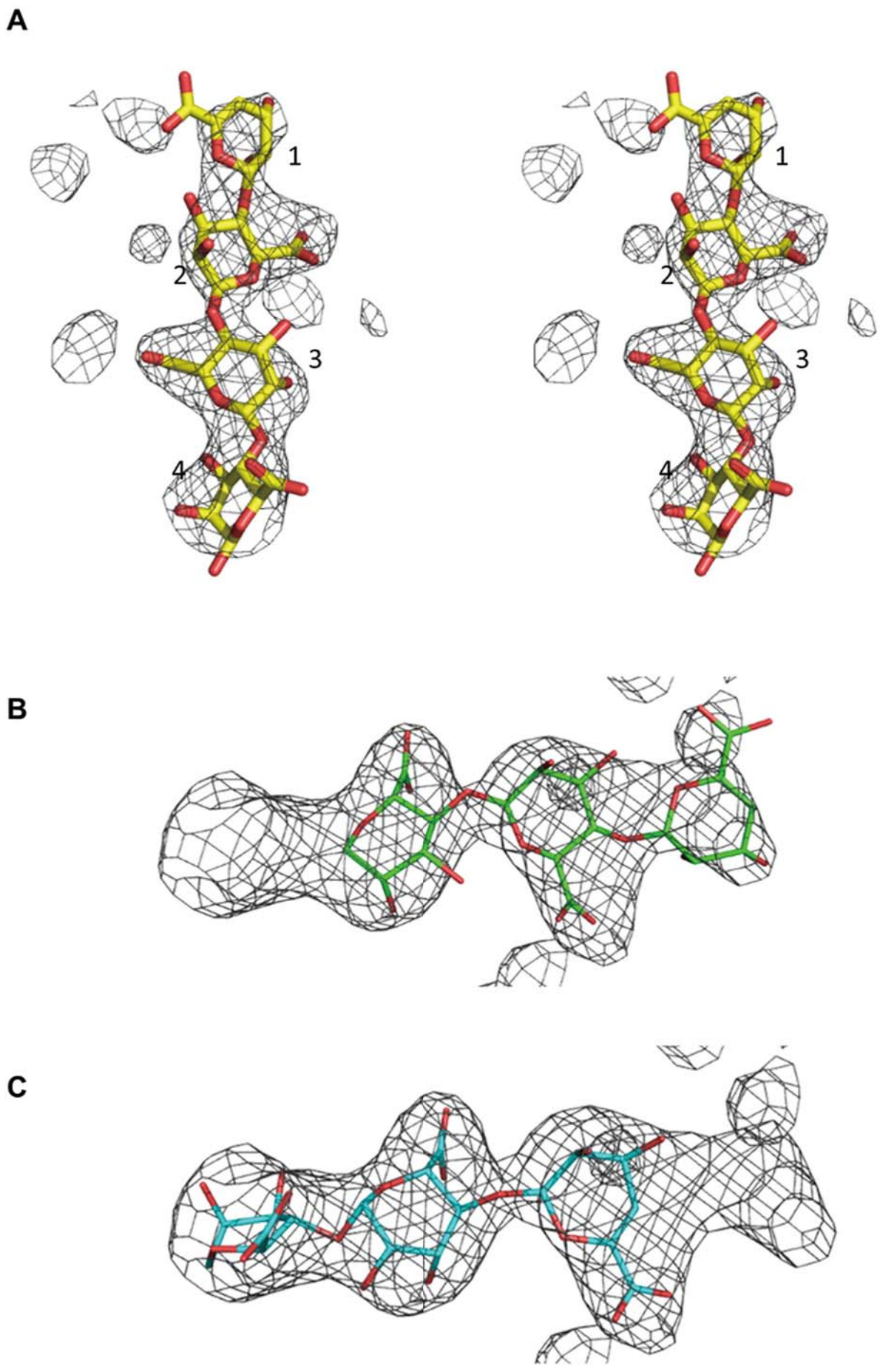

Figure 3

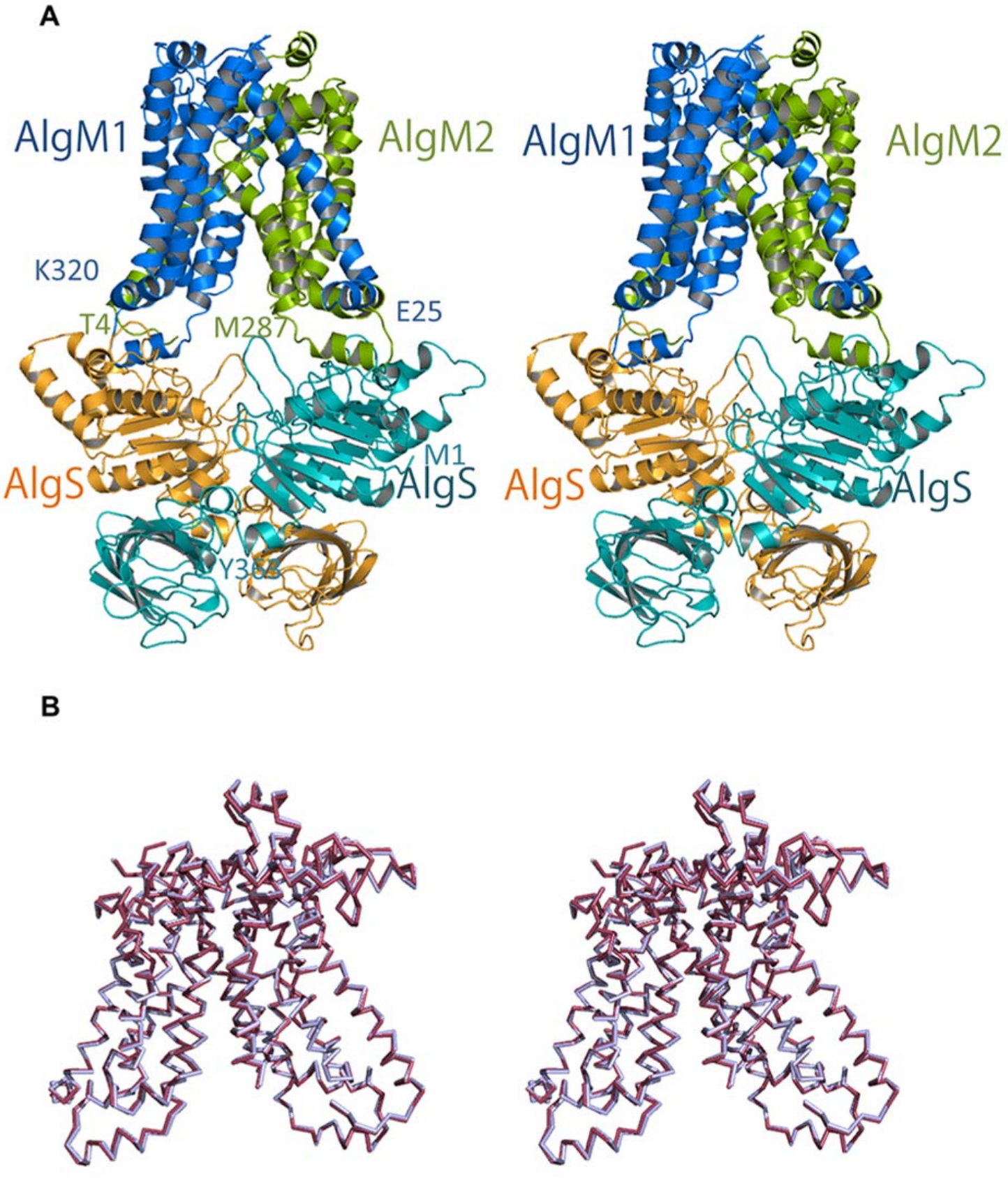
A
AlgM1
AlgM2
K320
T4
M287
E25
M1
AlgS
AlgS
Y382
AlgM1
AlgM2
AlgS
AlgS
B

Figure 4

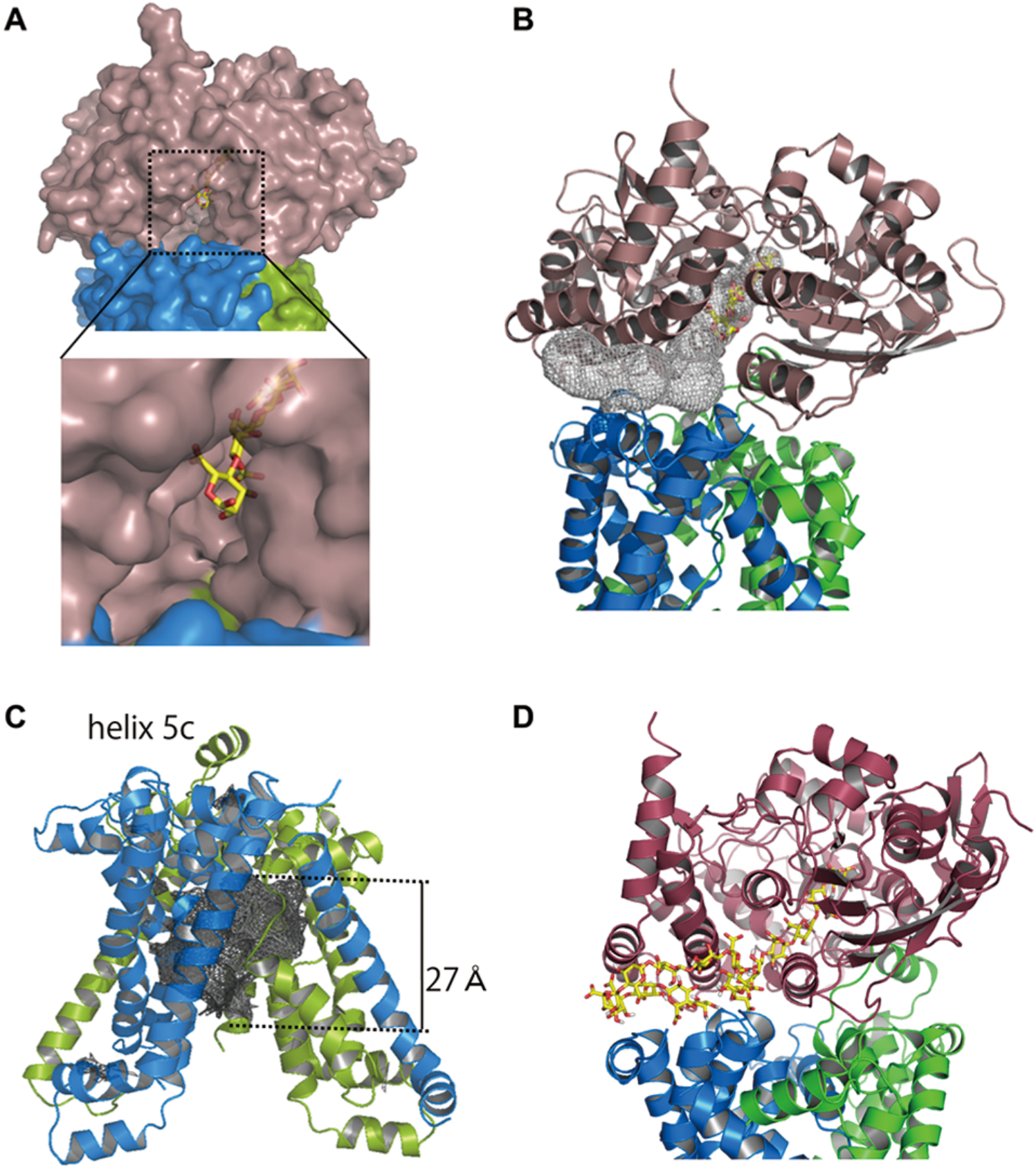

Figure 5

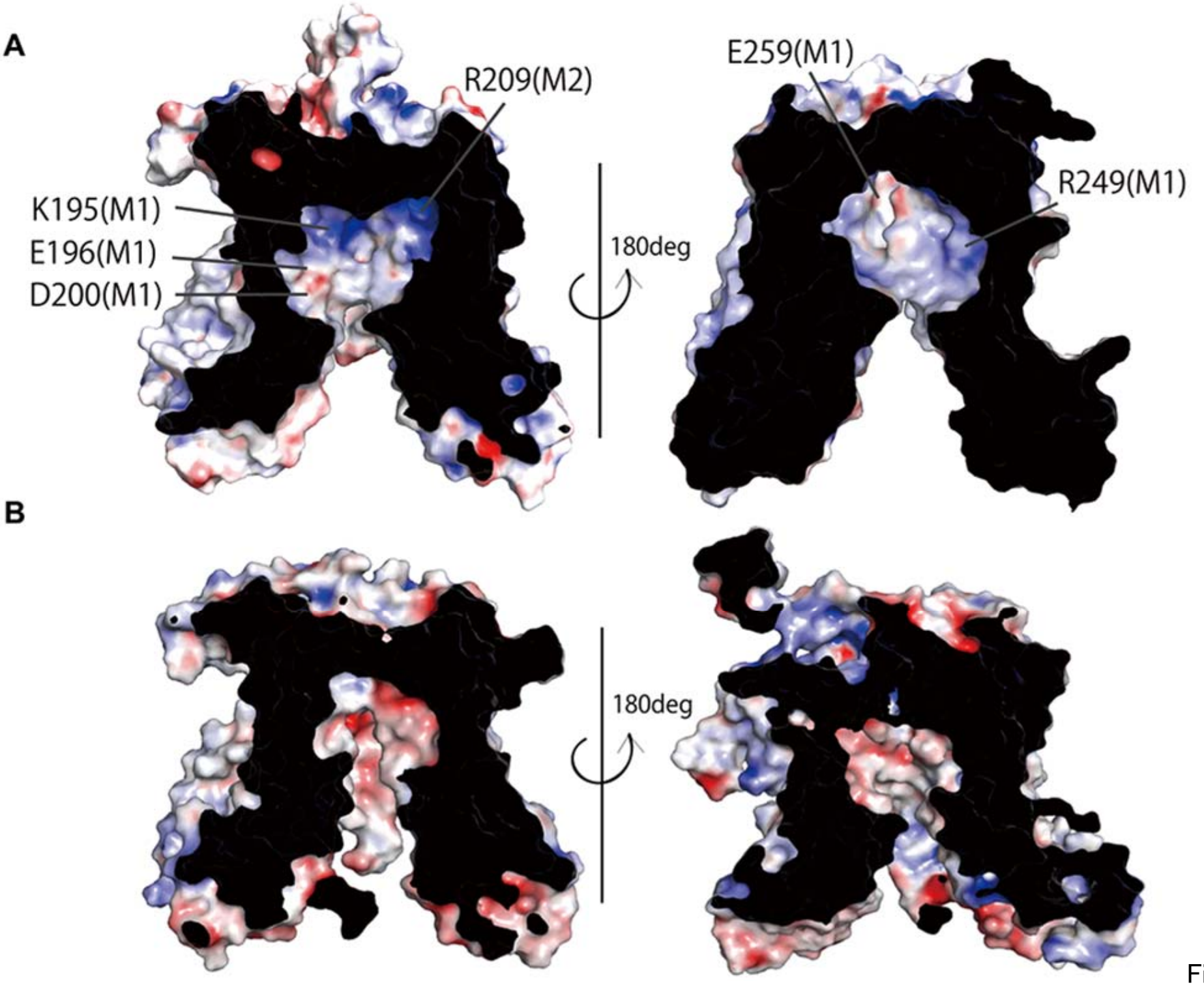
A
R209(M2)
K195(M1)
E196(M1)
D200(M1)
180deg
E259(M1)
R249(M1)
B
180deg

Figure 6

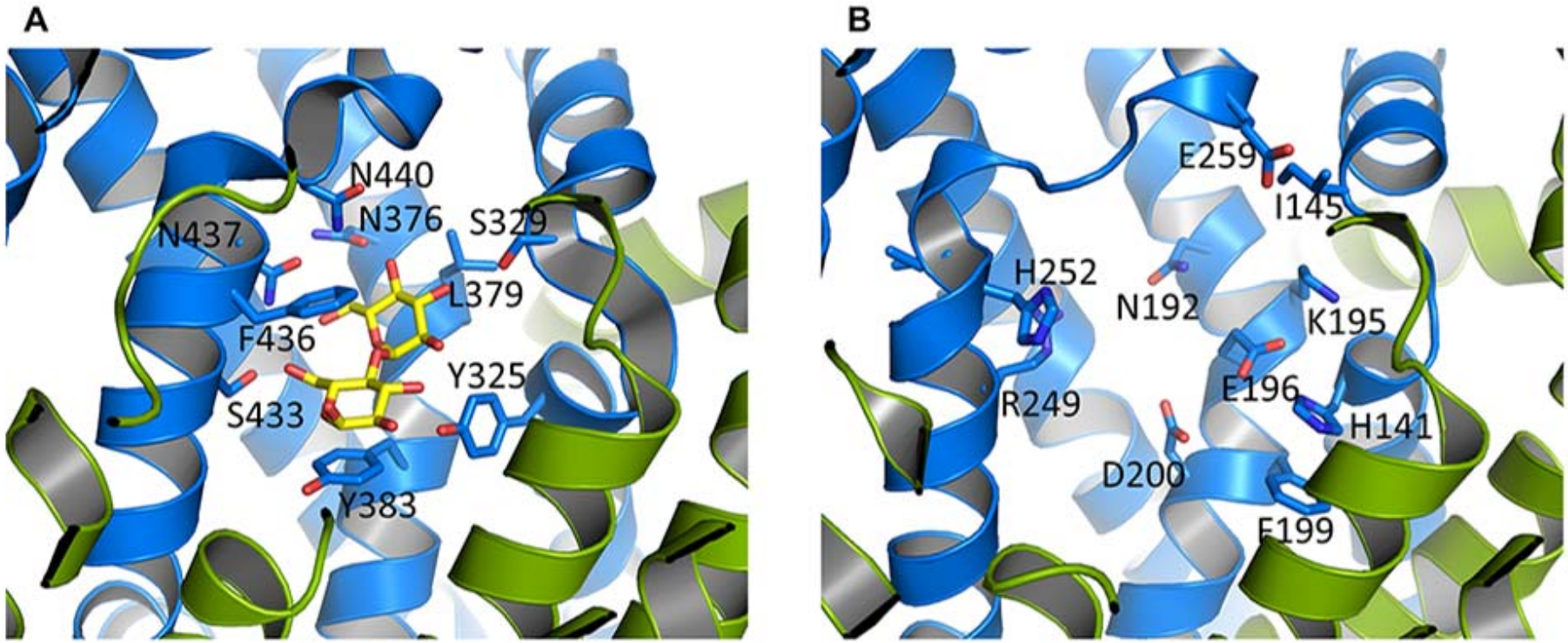
A
N440
N376
S329
N437
L379
F436
Y325
S433
Y383
B
E259
I145
H252
N192
K195
E196
R249
H141
D200
F199

Figure 7

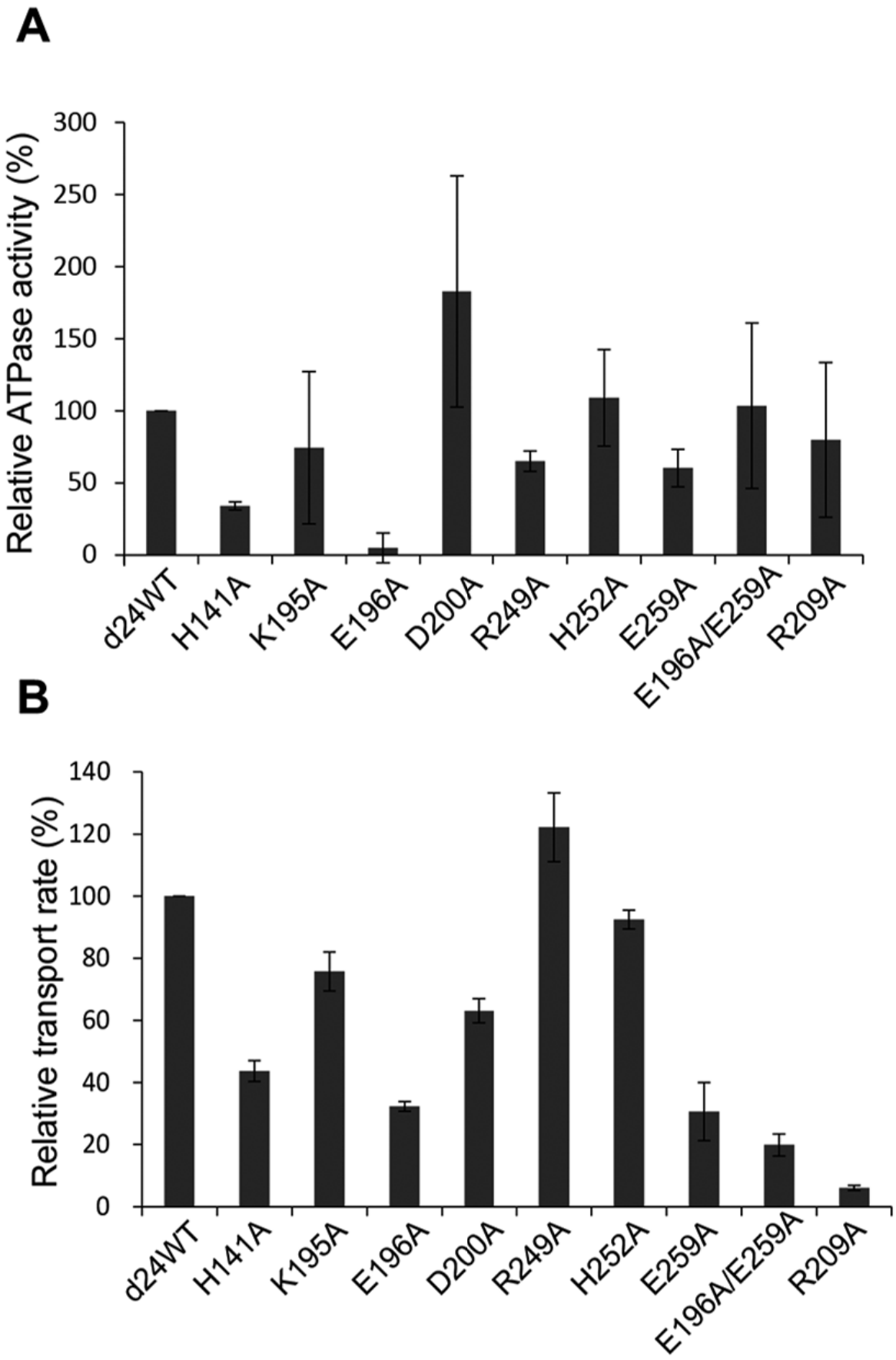
A
Relative ATPase activity (%)
300
250
200
150
100
50
0
d24WT
H141A
K195A
E196A
D200A
R249A
H252A
E259A
E196A/E259A
R209A
B
Relative transport rate (%)
140
120
100
80
60
40
20
0
d24WT
H141A
K195A
E196A
D200A
R249A
H252A
E259A
E196A/E259A
R209A

Figure 8

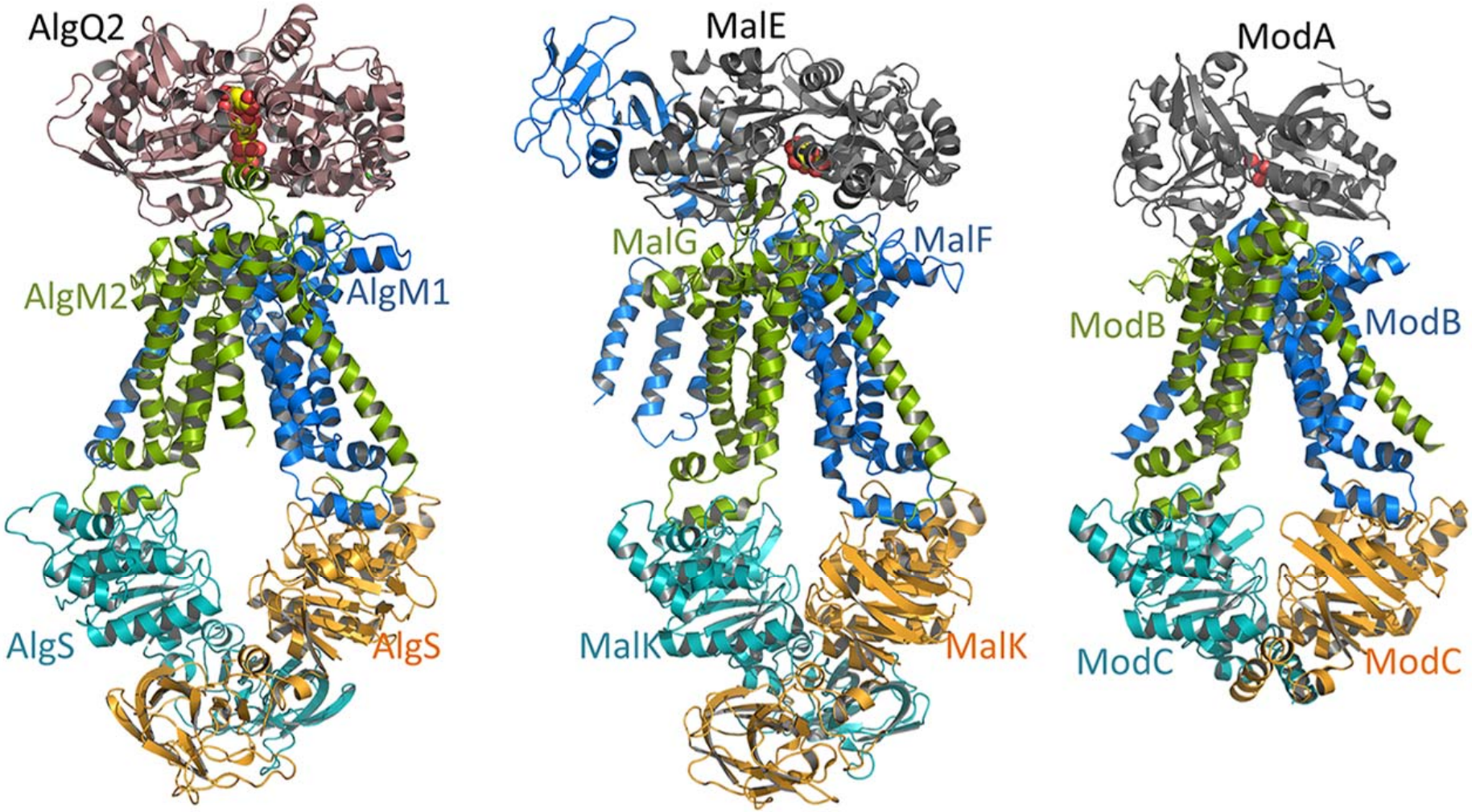

Alginate transporter

Maltose transporter
(PDB ID:3PV0)

Molybdate/tungstate
transporter
(PDB ID:2ONK)

Figure 9

Table 1: Crystallization conditions, data collection, and structure refinement

	AlgM1M2SS/AlgQ2	SeMet-AlgM1M2SS/AlgQ2	AlgM1M2SS
Crystallization conditions			
Sample solution	7 mg/mL AlgM1(d24)M2(H10)SS(E160Q), 3 mg/mL AlgQ2, 1 mM ΔMMM, 3.6 mM DM, 16 mM CHAPSO	7 mg/mL SeMet-AlgM1(d24)M2(H10)SS(WT), 3 mg/mL AlgQ2, 1 mM ΔMMM, 1.2 mM Cymal-6, 16 mM CHAPSO	10 mg/mL AlgM1(d24)M2(H10)SS(E160Q), 7 mg/mL AlgQ2, 2 mM ATP, 1.2 mM Cymal-6
Reservoir solution	18% PEG3000, 0.15 M NaCl, 0.1 M *N*-(2-acetamido)iminodiacetic acid (pH 6.6)	18% PEG4000, 0.15 M sodium potassium tartrate, 0.1 M *N*-(2-acetamido)iminodiacetic acid (pH 6.6)	22% PEG4000, 0.15 M sodium potassium tartrate, 0.1 M *N*-(2-acetamido)iminodiacetic acid (pH 6.6)
Data collection			
Wavelength (Å)	1.00000	0.97939	1.00000
Resolution range (Å)	30.0–3.2 (3.31–3.20) [a]	50.0–3.8 (3.94–3.80) [a]	30.0–4.5 (4.58–4.50) [a]
Space group	$P2_12_12_1$	$P2_12_12_1$	$P1$
Unit-cell parameters (Å, deg.)	a = 71.37, b = 134.18, c = 273.80	a = 71.82, b = 132.93, c = 271.57	a = 115.25, b = 151.19, c = 162.41, α = 68.66, β = 81.76, γ = 90.10
Total observations	157621	178605	119470
Unique reflections	43105	48893	57115
Completeness (%)	97.6 (96.1)	99.2 (98.8)	96.2 (91.4)
$I/\sigma(I)$	23.9 (3.2)	30.8 (8.0)	14.7 (1.3)
R_{merge}	0.089 (0.516)	0.084 (0.278)	0.049 (0.597)
Refinement			
Resolution range (Å)	30.0–3.2		30.0–4.5
R_{work}/R_{free}	0.233/0.279		0.279/0.319
No. atoms			
Protein	14154		40492
Alginate	48		-
Calcium ion	1		-
rmsd			
Bond lengths (Å)	0.005		0.004
Bond angles (deg.)	1.044		1.118
Ramachandran plot			
Most favored (%)	92.0		89.1
Allowed (%)	7.3		9.4
Outlier (%)	0.7		1.5

[a] The highest resolution shell is shown in parentheses.

Supplementary Experimental Procedures

Construction of Plasmids for the Overexpression of AlgM1M2SS

The overexpression systems for intact and truncated AlgM1M2SS with a His-tag (10 × His residues) were constructed in *E. coli* as follows. The strain A1 genome fragment was introduced into the expression vector pET21b or pET19b (Novagen). The vectors pET21b and pET19b are designed to express proteins with a hexahistidine (6 × His)-tagged sequence at the C-terminus and a decahistidine (10 × His)-tagged sequence at the N-terminus, respectively. The oligonucleotides used to construct the plasmids are listed in Table S3. The DNA fragment encoding AlgS-AlgM1-AlgM2 was amplified by polymerase chain reaction (PCR) using KOD plus polymerase (Toyobo) and strain A1 genomic DNA as the template. The amplicon was digested with *Nde*I and *Xho*I, then ligated with *Nde*I and *Xho*I-digested pET21b using Ligation High (Toyobo). The resulting plasmid containing the AlgS, AlgM1, and AlgM2 genes was designated pET21b-AlgM1(d0)M2(H6)SS(WT). To construct the plasmid for the overexpression of AlgM1M2SS with a His-tag at the N-terminus of AlgM1, the DNA fragment encoding AlgM1 and AlgM2 was amplified by PCR with strain A1 genomic DNA as the template. The amplified fragment was digested with *Nde*I and *Bam*HI and ligated with *Nde*I- and *Bam*HI-digested pET19b. The resulting plasmid was designated pET19b-AlgM1(d0, H10)M2. The plasmid pCOLADuet-1 (Merck)-AlgS containing the AlgS gene with the original start and stop codons was prepared in a similar manner. The pET19b and pCOLADuet-1 plasmids are compatible in *E. coli* cells. To enhance the purification efficiency, a DNA fragment encoding a tetrahistidine tag (4 × His) was inserted before the stop codon of the AlgM2 gene in pET21b-AlgM1(d0)M2(H6)SS(WT) by inverse PCR. After phosphorylation by T4 polynucleotide kinase (Toyobo), the amplified DNA

fragment was self-ligated using Ligation High. The resulting plasmid was designated pET21b-AlgM1(d0)M2(H10)SS(WT).

To prepare high-quality crystals, the truncated AlgM1M2SS was expressed in *E. coli*. Cytoplasmic disorder of the N-terminal region of the transmembrane protein AlgM1 was predicted by the programs TopPred (Von Heijne, 1992), PHD (Rost and Sander, 1993), prof (Rost et al., 1995), and GlobPlot (Linding, 2003). Based on the *in silico* prediction, two truncated forms [AlgM1(d24) and AlgM1(d33)] were constructed by genetic engineering. To construct the truncated forms of AlgM1, inverse PCR was performed using pET21b-AlgM1(d0)M2(H10)SS(WT) as the template. After phosphorylation with T4 polynucleotide kinase, the amplified DNA fragments were self-ligated with Ligation High. The resulting plasmids were designated pET21b-AlgM1(d24)M2(H10)SS(WT) and pET21b-AlgM1(d33)M2(H10)SS(WT), respectively.

To obtain an ATPase-deficient mutant of AlgM1M2SS, Glu160 of AlgS was replaced with Gln by site-directed mutagenesis. The site-directed mutagenesis was performed using pET21b-AlgM1(d0)M2(H10)SS(WT), pET21b-AlgM1(d24)M2(H10)SS(WT), or pET21b-AlgM1(d33)M2(H10)SS(WT) as the template and a QuikChange site-directed mutagenesis kit (Stratagene). The resulting plasmids were designated pET21b-AlgM1(d0)M2(H10)SS(E160Q), pET21b-AlgM1(d24)M2(H10)SS(E160Q), and pET21b-AlgM1(d33)M2(H10)SS(E160Q), respectively.

To prepare seven alanine mutants of AlgM1 (H141A, K195A, E196A, D200A, R249A, H252A, and E259A), one mutant of AlgM2 (R209A), and a double mutant of AlgM1 (E196A/E259A), 16 oligonucleotides were synthesized (Table S3). Site-directed mutagenesis was performed as described above using pET21b-

AlgM1(d24)M2(H10)SS(WT) as the template.

DNA Manipulations

Genomic DNA isolation, subcloning, transformation, and gel electrophoresis were performed as previously described (Sambrook et al., 1989). The nucleotide sequences of the ABC transporter genes were confirmed using the dideoxy-chain termination method with an automated DNA sequencer model 3730xl (Applied Biosystems) (Sanger et al., 1977). Restriction endonucleases and DNA-modifying enzymes were purchased from Takara Bio and Toyobo.

Expression and Purification of Proteins

E. coli BL21-Gold(DE3)/pLysS was used as the host strain for the expression of various types of AlgM1M2SS. The methionine auxotrophic *E. coli* strain B834(DE3) was used to prepare SeMet-substituted AlgM1M2SS. TB medium (Tartof and Hobbs, 1987) was used to culture BL21-Gold(DE3)/pLysS, and minimal medium containing SeMet (25 mg/mL) was used to culture B834(DE3). Cells were collected by centrifugation at 6,000 g and 4 °C for 5 min, suspended in a standard buffer [20 mM Tris-HCl (pH 8.0), 100 mM NaCl, 10 mM $MgCl_2$, and 10% glycerol], and ultrasonically disrupted (Insonator Model 201M, Kubota) for 20 min on ice. The supernatant fraction obtained after centrifugation at 20,000 g and 4 °C for 20 min to remove cell debris was further ultracentrifuged at 100,000 g and 4 °C for 1 h. The pelleted membranes were solubilized with 1% DDM (Dojindo) and loaded on a Ni-NTA column (Qiagen). After being washed with standard buffer containing 1 × critical micelle concentration (CMC) of detergent and 20 mM imidazole, the sample was eluted using a linear gradient of imidazole (20–200 mM). The proteins were confirmed by SDS-PAGE, combined, and concentrated by ultrafiltration. The sample was then applied to a HiLoad 16/60

Superdex 200 PG or Superdex 200 GL column (GE Healthcare Science) and eluted using standard buffer containing 2 × CMC of detergent. Detergent exchange was performed during protein purification at the affinity chromatography step. Purified AlgM1M2SS was concentrated to a final concentration of 10 mg/mL and stored at 4 °C. The AlgM1(d24)M2(H10)SS(WT) selenomethionine derivative was purified in the same manner, except that 5 mM 2-mercaptoethanol was added throughout the purification process. The purified protein concentration was determined using a bicinchoninic acid protein assay kit (Pierce).

AlgQ1 and AlgQ2 were expressed and purified as previously described (Nishitani et al., 2012).

Preparation of Alginate Derivatives

The alginate derivatives were prepared as previously described using *Eisenia bicyclis* sodium alginate (M/G ratio, 56.5/43.5%; average molecular mass, 300 kDa) (Nacalai Tesque) (Nishitani et al., 2012). The size of the oligosaccharide was confirmed by thin layer chromatography (TLC) (Hashimoto et al., 2000) and fluorophore-assisted carbohydrate electrophoresis (FACE) (Jackson, 1990) using 8-aminonaphthalene-1,3,6-trisulfonic acid. Longer oligoalginates designated as 8–20M or 8–20G were a mixture of oligomannuronates or oligoguluronates with degrees of polymerization of 8 to 20 that were fractionated by size exclusion chromatography (Bio gel P2, BioRad).

Crystallization and X-ray Analysis

AlgM1(d24)M2(H10)SS(E160Q) purified with DM was crystallized in the presence of AlgQ2 by sitting drop vapor diffusion in a 96 well plate. The protein was crystallized using 1 μL of sample solution containing 7 mg/mL importer, 3 mg/mL AlgQ2, 1 mM ΔMMM, and 16 mM CHAPSO in standard buffer containing DM and 1 μL of reservoir

solution comprising 18% polyethylene glycol (PEG) 3000, 0.15 M NaCl, and 0.1 M *N*-(2-acetamido)iminodiacetic acid (pH 6.6). The SeMet derivative of AlgM1(d24)M2(H10)SS(WT) purified with Cymal-6 was crystallized using 1 μL of sample solution comprising 7 mg/mL importer, 3 mg/mL AlgQ2, 1 mM unsaturated trimannuronate (ΔMMM), and 16 mM CHAPSO in standard buffer containing Cymal-6 and 1 μL of reservoir solution comprising 18% PEG4000, 0.15 M sodium potassium tartrate, and 0.1 M *N*-(2-acetamido) iminodiacetic acid (pH 6.6). Crystals of solute-binding protein-free AlgM1M2SS were unexpectedly obtained from the sample solution of 10 mg/mL AlgM1(d24)M2(H10)SS(E160Q) purified with Cymal-6, 7 mg/mL AlgQ2, and 2 mM ATP, although the composition of the sample solution was initially designed to form another conformation of AlgM1M2SS in complex with AlgQ2. The reservoir solution consisted of 22% PEG4000, 0.15 M sodium potassium tartrate, and 0.1 M *N*-(2-acetamido)iminodiacetic acid (pH 6.6).

Single crystals were soaked in a cryoprotectant solution containing 20% PEG200 or 20% glycerol and then frozen under a stream of cold nitrogen gas. The X-ray diffraction patterns from numerous crystals were examined using the SPring-8 BL38B1, BL41XU, and BL44XU beamlines. The X-ray diffraction data for the importer/AlgQ2 complex and solute-binding protein-free AlgM1M2SS were collected using a Quantum210 or Quantum315 CCD detector (Area Detector Systems Corporation) at the BL38B1 beamline. The diffraction data were indexed, integrated, and scaled using the HKL2000 program (Otwinowski and Minor, 1997).

The structure of the complex of AlgM1M2SS and AlgQ2 was initially determined by the molecular replacement method with Molrep (Vagin and Teplyakov, 2010) using the coordinates of AlgQ2 with tetrasaccharide (PDB ID, 1J1N) and with

Amore (Navaza, 1994) using each subunit of the maltose transporter, MalF, MalG, and MalK (PDB ID, 2R6G). The anomalous cross-Fourier electron density obtained from the data set for the SeMet derivative was used for detailed model building with the program Coot (Emsley and Cowtan, 2004). The structure of binding protein-free AlgM1M2SS was determined with the program Amore using the structure of the transporter tetramer (AlgM1M2SS) in the complex of AlgM1M2SS and AlgQ2. The programs CNS (Brünger et al., 1998) and Phenix (Adams et al., 2010) were used for the structure refinement. A random selection of 5% of the reflections were excluded from refinement and used to calculate R_{free}. After each cycle of refinement, the model was adjusted manually using Coot. Figures showing the protein structure were prepared using Pymol (Schrödinger, 2013) and Caver (Chovancova et al., 2012).

Docking simulation

Interaction of hexadecamannuronate (16 residues) with the tunnel-like structure formed at the interface between AlgQ2 and AlgM1M2 was simulated by *AutoDock Vina* (Trott and Olson, 2010). The coordinates of oligomannuronate were prepared using Coot. The grid was set to cover the tunnel of AlgQ2 and the interface between AlgQ2 and AlgM1M2 (size_x = 45.0, size_y = 40.5, size_z = 30.8). Figures for docking forms obtained by the simulation were prepared using Pymol.

Supplementary References

Adams, P.D., Afonine, P.V., Bunkóczi, G., Chen, V.B., Davis, I.W., Echols, N., Headd, J.J., Hung, L.W., Kapral, G.J., Grosse-Kunstleve, R.W., et al. (2010). PHENIX: a comprehensive Python-based system for macromolecular structure solution. Acta Crystallogr. D Biol. Crystallogr. *66*, 213–221.

Brünger, A.T., Adams, P.D., Clore, G.M., DeLano, W.L., Gros, P., Grosse-Kunstleve, R.W., Jiang, J.S., Kuszewski, J., Nilges, M., Pannu, N.S., et al. (1998). Crystallography & NMR system: A new software suite for macromolecular structure determination. Acta Crystallogr. D Biol. Crystallogr. *54*, 905–921.

Chovancova, E. Pavelka, A., Benes, P., Strnad, O., Brezovsky, J., Kozlikova, B., Gora, A., Sustr, V., Klvana, M., Medek, P., et al. (2012). CAVER 3.0: a tool for the analysis of transport pathways in dynamic protein structures. PLoS Comput. biol. *8*, e1002708

Emsley, P., and Cowtan, K. (2004). Coot: model-building tools for molecular graphics. Acta Crystallogr. D Biol. Crystallogr. *60* 2126–21232.

Hashimoto, W., Miyake, O., Momma, K., Kawai, S., and Murata, K. (2000). Molecular identification of oligoalginate lyase of *Sphingomonas* sp. strain A1 as one of the enzymes required for complete depolymerization of alginate. J. Bacteriol. *182*, 4572–4577.

Jackson, P. (1990). The use of polyacrylamide-gel electrophoresis for the high-resolution separation of reducing saccharides labelled with the fluorophore 8-aminonaphthalene-1,3,6-trisulphonic acid. Detection of picomolar quantities by an imaging system based on a cooled cha. Biochem. J. *270*, 705–713.

Linding, R. (2003). GlobPlot: exploring protein sequences for globularity and disorder. Nucleic Acids Res. *31*, 3701–3708.

Navaza, J. (1994). AMoRe: an automated package for molecular replacement. Acta Crystallogr. A Found. Crystallogr. *50*, 157–163.

Nishitani, Y., Maruyama, Y., Itoh, T., Mikami, B., Hashimoto, W., and Murata, K. (2012). Recognition of heteropolysaccharide alginate by periplasmic solute-binding proteins of a bacterial ABC transporter. Biochemistry *51*, 3622–3633.

Otwinowski, Z., and Minor, W. (1997). Processing of x-ray diffraction data collected in oscillation mode. Methods Enzymol. *276*, 307–326.

Rost, B., and Sander, C. (1993). Prediction of protein secondary structure at better than 70% accuracy. J. Mol. Biol. *232*, 584–599.

Rost, B., Casadio, R., Fariselli, P., and Sander, C. (1995). Transmembrane helices predicted at 95% accuracy. Protein Sci. *4*, 521–533.

Sambrook, J., Fritsch, E.F., and Maniatis, T. (1989). Molecular Cloning: A Laboratory Manual, 2nd edit. (NewYork: Cold Spring Harbor Laboratory Press).

Sanger, F., Nicklen, S., and Coulson, A.R. (1977). DNA sequencing with chain-terminating inhibitors. Proc. Natl. Acad. Sci. USA *74*, 5463–5467.

Schrödinger, L.L.C. (2013). The PyMOL Molecular Graphics System, Version 1.6.0.0.

Tartof, K.D., and Hobbs, C.A. (1987). Improved media for growing plasmid and cosmid clones. Bethesda Res. Lab. Focus *9*, 12.

Trott, O., and Olson, A.J. (2010). AutoDock Vina: improving the speed and accuracy of docking with a new scoring function, efficient optimization, and multithreading. J. Comput. Chem. *31*, 455-461.

Vagin, A., and Teplyakov, A. (2010). Molecular replacement with MOLREP. Acta Crystallogr. D Biol. Crystallogr. *66*, 22–25.

von Heijne, G. (1992). Membrane protein structure prediction. Hydrophobicity analysis and the positive-inside rule. J. Mol. Biol. *225*, 487–494.

Supplementary Figure Legends

Figure S1, related to Figure 1: Characteristics of strain A1 and alginate.

(A) Diagram of alginate uptake and degradation in strain A1. Pit on cell surface, alginate-binding proteins (AlgQ1 and AlgQ2), inner membrane ABC transporter (AlgM1, AlgM2, and AlgS), cytoplasmic endotype alginate lyases (A1-I which is autocatalytically divided into A1-II and A1-III), and exotype alginate lyase (A1-IV) are illustrated. The gene cluster involved in alginate uptake and degradation is also shown. AlgO is an alginate-dependent transcriptional regulator.

(B) Transmission electron microscope image of strain A1*. An arow indicates the "pit" formed on the cell surface dependent on extracellular alginate.

(C) Structure of some oligoalginate derivatives used in this study.

*Reprinted from Biochem. Biophys. Res. Commun., 220(3), pp981, Hisano, T., Kimura, N., Hashimoto, W., and Murata, K. Pit structure on bacterial cell surface. Copyright (1996), with permission from Elsevier.

Figure S2, related to Figure 1: ATPase activity and transport rate of AlgM1M2SS.

Unless otherwise stated, saccharides were added at a final concentration of 20 μM.

(A) Relative ATPase activity of reconstituted AlgM1(d0)M2(H10)SS(WT) with and without a solute-binding protein (AlgQ2) and/or oligoalginate (ΔMMM). ATPase activity of AlgM1M2SS in the presence of AlgQ2 and ΔMMM is taken as 100%. The experiments are repeated twice.

(B) Relative ATPase activity of reconstituted AlgM1(d24)M2(H10)SS(WT) using AlgQ2 and labeled or non-labeled oligoalginate (n = 3~20). ATPase activity of AlgM1M2SS using ΔMMM as a substrate is taken as 100%.

(C) Relative PA-ΔMMMM transport rate of AlgM1(d24)M2(H10)SS(WT) with and without AlgQ2 and/or ATP. Transport rate of AlgM1M2SS in the presence of AlgQ2 and ATP is taken as 100%. The experiments are repeated three times.

(D) A typical time course of PA-ΔMMMM transport by AlgM1(d24)M2(H10)SS(WT). AlgQ2 was used as a solute-binding protein.

(E) ΔMMM-dependent ATPase activity of AlgM1(d0)M2(H10)SS(WT) in the detergent (0.045% Cymal-6 and 0.25% CHAPSO). The experiments are repeated three times.

Figure S3, related to Figure 2: Model accuracy and structural characterization of AlgM1M2.

(A) Wall-eyed stereo diagram of the overall structure and 2|Fo|-|Fc| density map of AlgM1M2SS complexed with AlgQ2 contoured at 1.5 σ. Pink, AlgQ2; blue, AlgM1; green AlgM2; orange and cyan, AlgS.

(A) Anomalous cross-Fourier electron density (black, contoured at 4 σ) using the data set of the SeMet-derivative. Methionine residues in the AlgM1M2SS model are represented as red sticks.

(B) Secondary structure elements of AlgM1.

(C) Secondary structure elements of AlgM2.

Figure S4, related to Figure 4: Structure of the binding protein-free form of the ABC transporter AlgM1M2SS.

Wall-eyed stereo diagram of the overall structure and 2|Fo|-|Fc| density map of AlgM1M2SS contoured at 1.5 σ. Blue, AlgM1; green AlgM2; orange and cyan, AlgS.

Figure S1, related to Figure 1

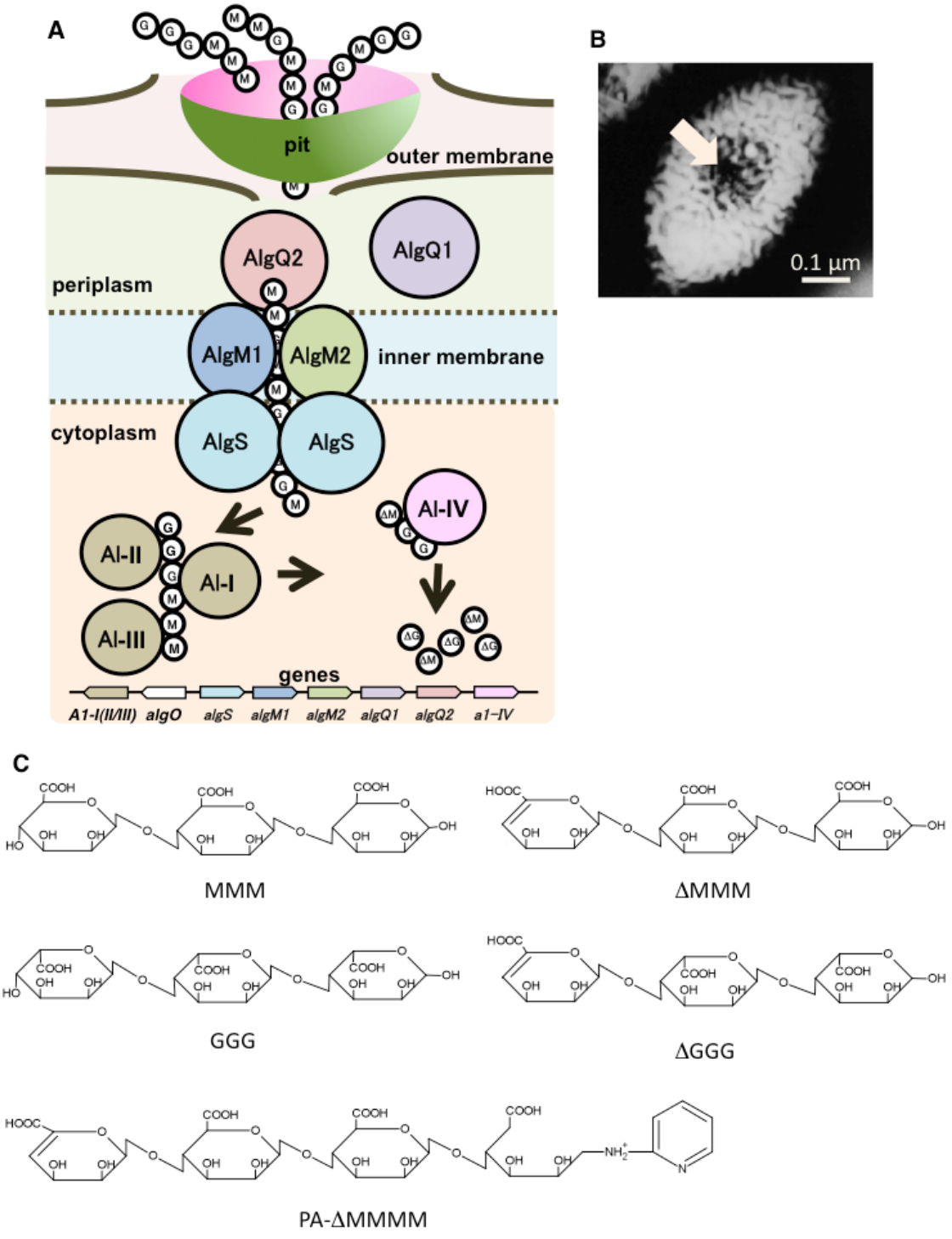

Figure S3, related to Figure 2

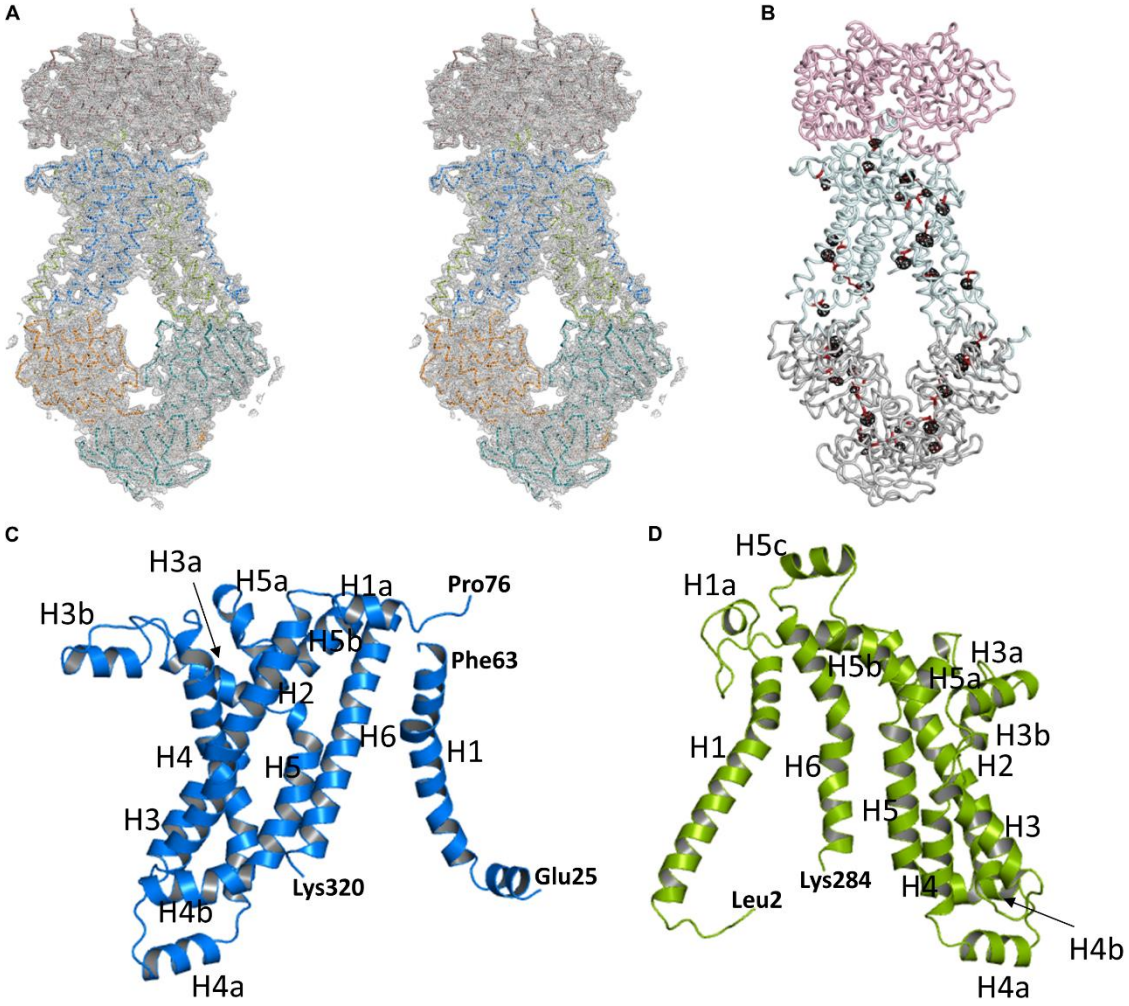

Figure S2, related to Figure 1

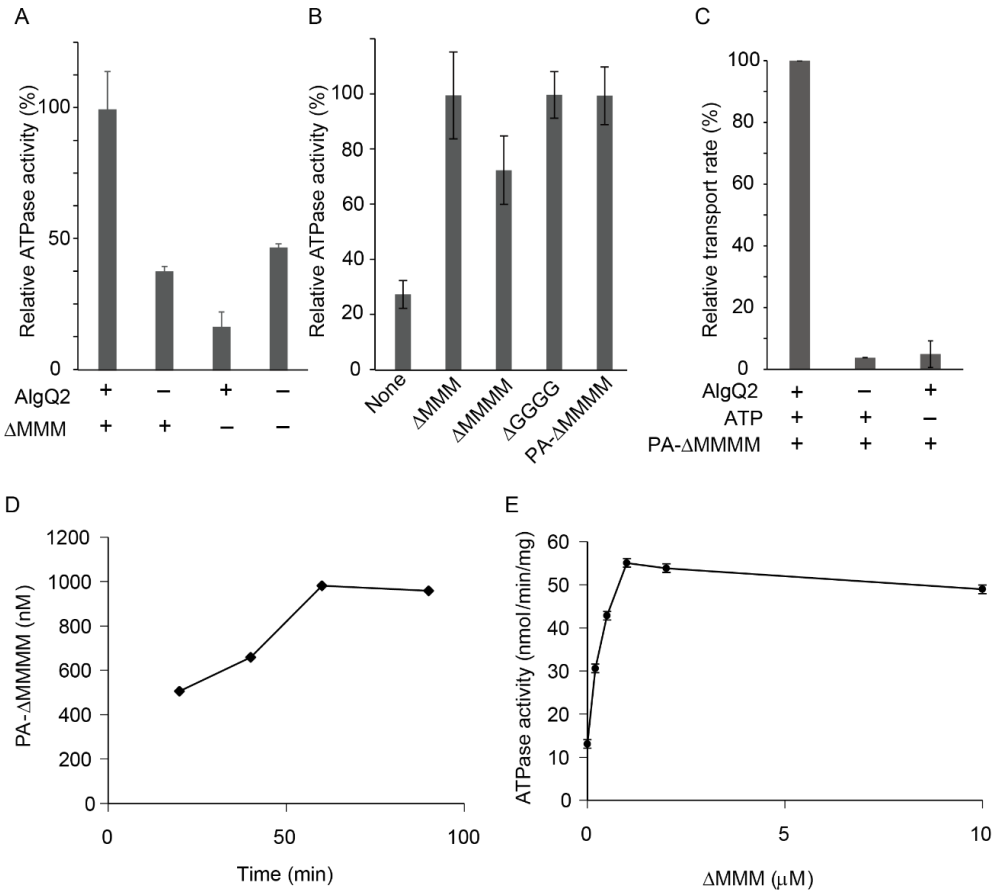

Figure S4, related to Figure 4

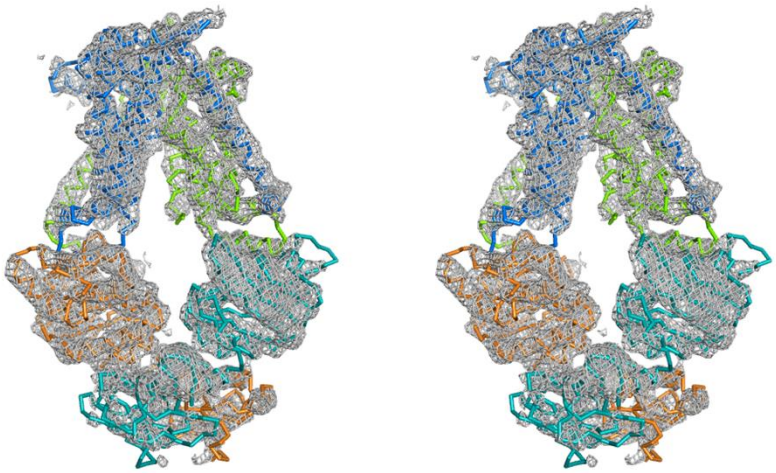

Table S1, related to Figrue 2: The rmsd between AlgQ2-bound AlgM1M2SS and type I ABC transporters

Reference subunits in AlgQ2-bound AlgM1M2SS	Matching molecules (PDB ID)						
	AlgQ2-free M1M2SS	**MetNI (3TUZ)**	**ModABC (2ONK)**	**ModBC (3D31)**	**MalEFGK2 (2R6G)**	**MalEFGK2 (3PV0)**	**MalFGK2 (3FH6)**
M1M2SS	0.75 (1278)	3.06 (821)	3.28 (947)	3.72 (859)	4.21 (872)	3.50 (1051)	2.74 (1049)
M1M2	0.47 (558)	3.42 (358)	3.10 (435)	3.33 (424)	4.25 (442)	2.88 (473)	2.37 (446)
M1	0.32 (283)	2.56 (194)	3.01 (227)	3.13 (223)	3.28 (187)	2.49 (235)	2.48 (216)
M2	0.50 (275)	3.25 (164)	3.08 (210)	2.98 (192)	2.45 (207)	2.44 (237)	2.13 (226)
SS	0.62 (726)	2.60 (457)	2.96 (423)	3.72 (438)	3.84 (532)	2.87 (646)	2.16 (676)
S	0.42 (363)	1.97 (263)	1.61 (221)	1.94 (243)	2.26 (331)	1.62 (345)	1.72 (340)

Numbers of Cα atoms used to calculate the rmsd are in the parentheses.

Table S2, related to experimental procedures: Oligonucleotides used in this study

Construct	Primer type	Sequence*
pET21b-AlgM1(d0)M2(H6)SS(WT)	sense	5’-GGCATATGGTAGCAAGCGTCAGCATTCAG-3’
	antisense	5’-GGCTCGAGTTCTTTTACGCCTCCGAGCATC-3’
pET19b-AlgM1(H6)M2	sense	5’-GGCATATGACAAGCGCCACCAAGGCACAG-3’
	antisense	5’-CCGGATCCTTATTCTTTTACGCCTCCGAGC-3’
pET21b-AlgS	sense	5’-GGCATATGGTAGCAAGCGTCAGCATTCAGA-3’
	antisense	5’-GGCTCGAGTCAGTAAATAGAGGCCTGTGAC-3’
pET21b-AlgM1(H6)M2SS(WT)	sense	5’-GGTCTAGAAATAATTTTGTTTAACTTTAAGGAG-3’
	antisense	5’-GGTCTAGAAATAATTTTGTTTAACTTTAAGGAG-3’
pET21b-AlgM1(d0)M2(H10)SS(WT)	sense	5’-TCAGTGGTGGTGGTGGTGGTGGTGGTGGTGCTCGAGTTCTTTTACGCCTCCGAGCATCACAC-3’
	antisense	5’-GATCCGGCTGCTAACAAAGCCCGAAAGGAAG-3’
pET21b-AlgM1(d24)M2(H10)SS(WT)	sense	5’-GAACGCCTGTGGAAAGACATCAAACGCG-3’
	antisense	5’-CATGGTGCTCCTCCTCGCCCGCAGCAAC-3’
pET21b-AlgM1(d33)M2(H10)SS(WT)	sense	5’-GACTGGCTGTTGTATGCCATGTTGCTAC-3’
	antisense	5’-CATGGTGCTCCTCCTCGCCCGCAGCAAC-3’
pET21b-AlgM1(d24)M2(H10)SS(E160Q)	sense	5’-GAAGGTCTTCCTCTTCGACCAGCCGCTCTCCAACCTCGAC-3’
	antisense	5’-GTCGAGGTTGGAGAGCGGCTGGTCGAAGAGGAAGACCTTC-3’
pET21b-AlgM1(d24/H141A)M2(H10)SS(WT)	sense	5’-CCATCGTCTATCTGCCTGCCTTCATCTCCATCGTGATC-3’
	antisense	5’-GATCACGATGGAGATGAAGGCAGGCAGATAGACGATGG-3’
pET21b-AlgM1(d24/K195A)M2(H10)SS(WT)	sense	5’-CTCGAACATCTGGGCGGAAGCGGGCTTC-3’
	antisense	5’-GAAGCCCGCTTCCGCCCAGATGTTCGAG-3’
pET21b-AlgM1(d24/E196A)M2(H10)SS(WT)	sense	5’-CTCGAACATCTGGAAGGCAGCGGGCTTCGATTCGATC-3’
	antisense	5’-GATCGAATCGAAGCCCGCTGCCTTCCAGATGTTCGAG-3’
pET21b-AlgM1(d24/D200A)M2(H10)SS(WT)	sense	5’-GGAAGCGGGCTTCGCTTCGATCGTGTATC-3’
	antisense	5’-GATACACGATCGAAGCGAAGCCCGCTTCC-3’
pET21b-AlgM1(d24/R249A)M2(H10)SS(WT)	sense	5’-GTGCTGCTGGTGATCGCCCTGGGCCACATCCTG-3’
	antisense	5’-CAGGATGTGGCCCAGGGCGATCACCAGCAGCAC-3’
pET21b-AlgM1(d24/H252A)M2(H10)SS(WT)	sense	5’-GTGATCCGCCTGGGCGCCATCCTGGAAGTGGG-3’
	antisense	5’-CCCACTTCCAGGATGGCGCCCAGGCGGATCAC-3’
pET21b-AlgM1(d24/E259A)M2(H10)SS(WT)	sense	5’-CTGGAAGTGGGCTTCGCGTACATCATCCTGCTG-3’
	antisense	5’-CAGCAGGATGATGTACGCGAAGCCCACTTCCAG-3’
pET21b-AlgM1(d24)M2(H10/R209A)SS(WT)	sense	5’-CTGCGCCATCTCTGCCTGGAACGGTTAC-3’
	antisense	5’-GTAACCGTTCCAGGCAGAGATGGCGCAG-3’

*Underlines are recognition sites by restriction enzymes.